Cell Metabolism

Article

Maternal circadian rhythms during pregnancy dictate metabolic plasticity in offspring

Graphical abstract

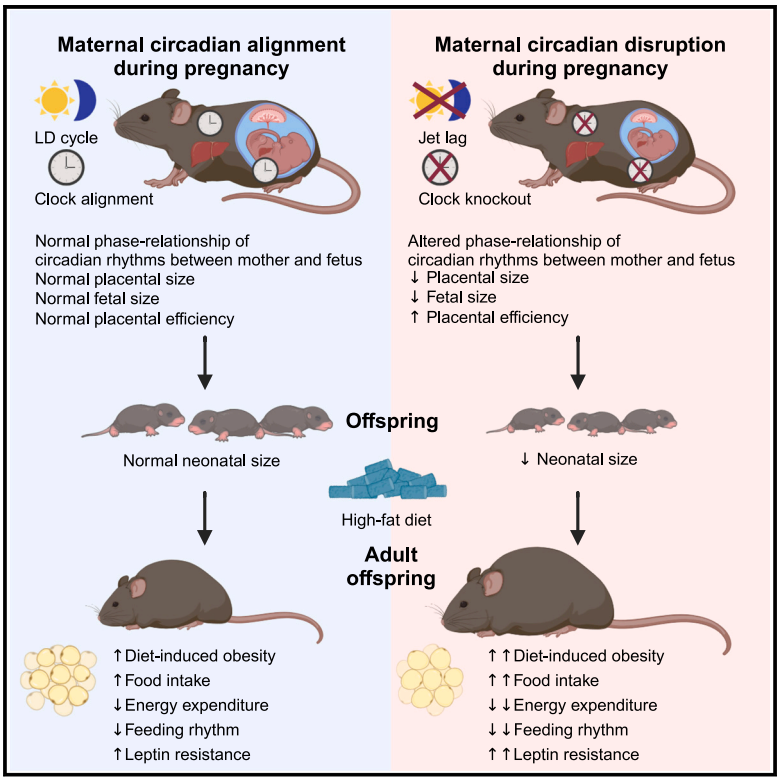

Highlights

- Circadian rhythm disruption during pregnancy (CRD-P) predisposes offspring to DIO
- Hepatic circadian reprogramming by high-fat diet is rewired by CRD-P
- CRD-P alters placental efficiency and the phase-relationship between mother and fetus
- Circadian alignment of CR in offspring prevents DIO exacerbation due to CRD-P

Authors

Na Yao, Kenichiro Kinouchi, Manami Katoh, ..., Pierre Baldi, Kaori Hayashi, Hiroshi Itoh

Correspondence

ken-k@keio.jp (K.K.),
hiito@keio.jp (H.I.)

In brief

Yao et al. demonstrate that maternal circadian rhythms during pregnancy impact placental signature and fetal rhythm. Diet-induced obesity in offspring is exacerbated by *in utero* chronodisruption. The obesity exacerbation is not fully prevented by temporal feeding restriction but is counteracted by caloric restriction with daily food replacement.

Yao et al., 2025, Cell Metabolism *37*, 395–412
February 4, 2025
https://doi.org/10.1016/j.cmet.2024.12.002

CellPress

Cell Metabolism

CellPress
OPEN ACCESS

Article

Maternal circadian rhythms during pregnancy dictate metabolic plasticity in offspring

Na Yao,[1] Kenichiro Kinouchi,[1,15,*] Manami Katoh,[2,13] Kousha Changizi Ashtiani,[3] Sherif Abdelkarim,[3] Hiroyuki Morimoto,[4] Takuto Torimitsu,[1] Takahide Kozuma,[1] Akihide Iwahara,[1] Shotaro Kosugi,[1,5] Jin Komuro,[6] Kyosuke Kato,[1] Shun Tonomura,[1] Toshifumi Nakamura,[1] Arata Itoh,[1] Shintaro Yamaguchi,[1] Jun Yoshino,[1,7,8] Junichiro Irie,[1] Hisayuki Hashimoto,[6] Shinsuke Yuasa,[6,9] Akiko Satoh,[10,11] Yohei Mikami,[12] Shusaku Uchida,[4] Takatoshi Ueki,[4] Seitaro Nomura,[2,13] Pierre Baldi,[3] Kaori Hayashi,[1] and Hiroshi Itoh[1,14,*]

[1]Division of Endocrinology, Metabolism, and Nephrology, Department of Internal Medicine, Keio University School of Medicine, Tokyo, Japan
[2]Department of Cardiovascular Medicine, Graduate School of Medicine, The University of Tokyo, Tokyo, Japan
[3]Department of Computer Science, University of California, Irvine, Irvine, CA 92697, USA
[4]Department of Integrative Anatomy, Nagoya City University Graduate School of Medical Sciences, Nagoya, Japan
[5]Health Center, Keio University, Yokohama, Japan
[6]Department of Cardiology, Keio University School of Medicine, Tokyo, Japan
[7]Division of Nephrology, Department of Internal Medicine, Faculty of Medicine, Shimane University, Izumo, Japan
[8]The Center for Integrated Kidney Research and Advance (IKRA), Faculty of Medicine, Shimane University, Izumo, Japan
[9]Department of Cardiovascular Medicine, Academic Field, Dentistry and Pharmaceutical Sciences, Okayama University, Okayama, Japan
[10]Department of Integrative Physiology, Institute of Development, Aging and Cancer, Tohoku University, Sendai, Japan
[11]Department of Integrative Physiology, National Center for Geriatrics and Gerontology, Obu, Japan
[12]Division of Gastroenterology and Hepatology, Department of Internal Medicine, Keio University School of Medicine, Tokyo, Japan
[13]Department of Frontier Cardiovascular Science, Graduate School of Medicine, The University of Tokyo, Tokyo, Japan
[14]Center for Preventive Medicine, Keio University, Tokyo, Japan
[15]Lead contact
*Correspondence: ken-k@keio.jp (K.K.), hiito@keio.jp (H.I.)
https://doi.org/10.1016/j.cmet.2024.12.002

SUMMARY

Tissue-level oscillation is achieved by tissue-intrinsic clocks along with network-dependent signals originating from distal organs and organismal behavior. Yet, it remains unexplored whether maternal circadian rhythms during pregnancy influence fetal rhythms and impact long-term susceptibility to dietary challenges in offspring. Here, we demonstrate that circadian disruption during pregnancy decreased placental and neonatal weight yet retained transcriptional and structural maturation. Intriguingly, diet-induced obesity was exacerbated in parallel with arrhythmic feeding behavior, hypothalamic leptin resistance, and hepatic circadian reprogramming in offspring of chronodisrupted mothers. *In utero* circadian desynchrony altered the phase-relationship between the mother and fetus and impacted placental efficiency. Temporal feeding restriction in offspring failed to fully prevent obesity, whereas the circadian alignment of caloric restriction with the onset of the active phase virtually ameliorated the phenotype. Thus, maternal circadian rhythms during pregnancy confer adaptive properties to metabolic functions in offspring and provide insights into the developmental origins of health and disease.

INTRODUCTION

The circadian rhythm is a nearly 24-h period of self-sustainable variation under constant conditions, which helps maintain homeostasis by predicting changes in the environmental light-dark (LD) cycle. This is primarily driven by the circadian clock, which governs an extensive array of biological rhythms.[1] A fundamental property of the circadian clock is its autonomous yet entrainable oscillations, which enable organisms to synchronize with their environmental cycles.[2] The central clock in the suprachiasmatic nucleus (SCN) is reset by light, whereas the peripheral clock is entrained by feeding and exercise, among other cues.[3] Emerging evidence showed that daily rhythms in a given tissue are subject to cyclic inputs from organismal behaviors and remote organs, such that tissue-intrinsic clocks integrate metabolic cycles to generate robust oscillations.[4] Hence, the distal coordination of circadian rhythms is considered a key aspect of metabolic homeostasis.

Whereas inherent genetic variations are linked to the adaptive capacity to the external environment and disease susceptibility, environment and nutrition during early life stages, including the gestational and postnatal periods, remarkably influence long-term health outcomes.[5,6] Low birth weight is associated with non-communicable diseases, such as diabetes and obesity.[7,8] The concept of the developmental origins of health and disease (DOHaD) prompted us to investigate whether maternal circadian

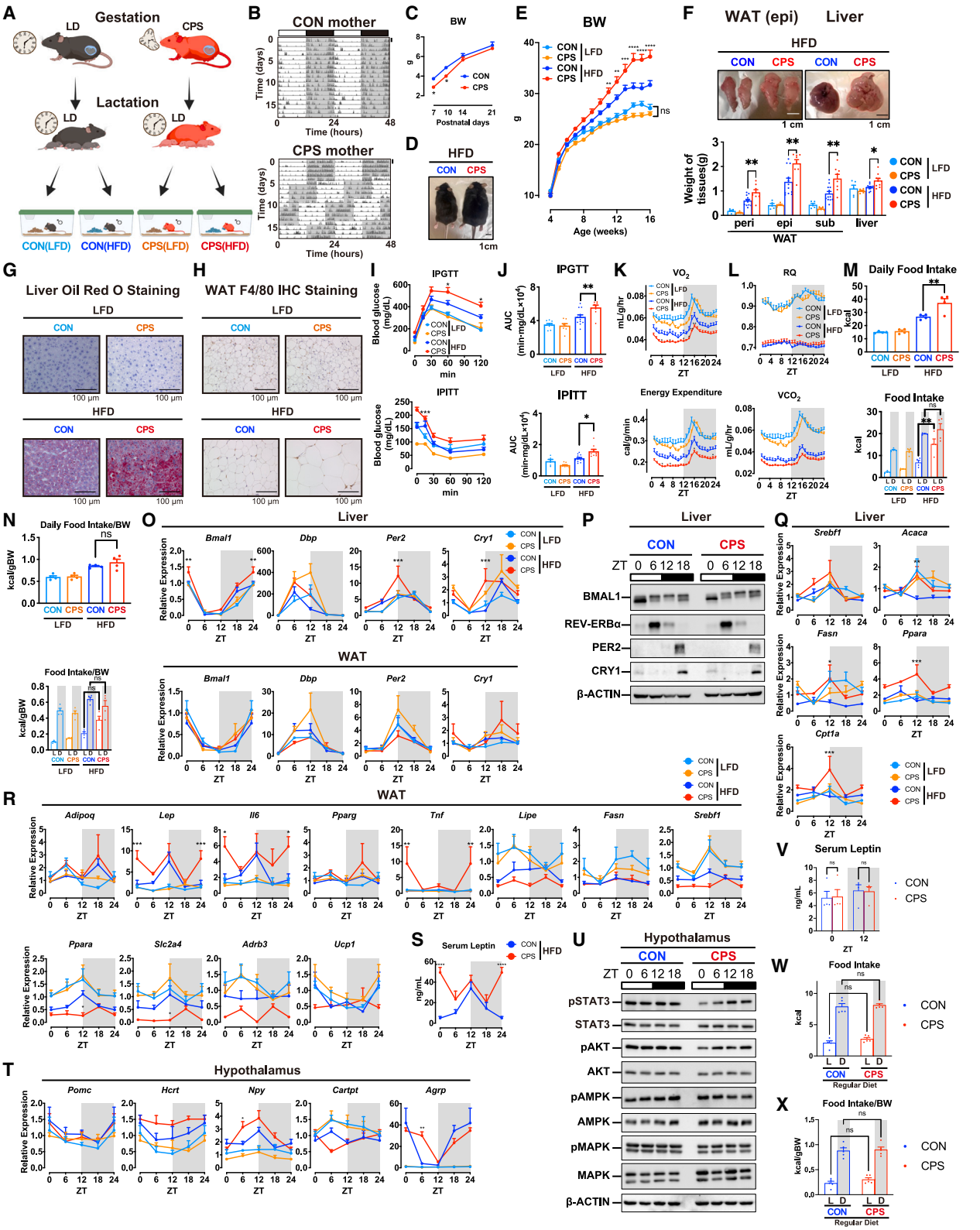

Figure 1. CPS during pregnancy promotes DIO in offspring

(A) Scheme for CPS during pregnancy and *ad libitum* HFD- or LFD-fed offspring mice born to CON and CPS mothers (CON(LFD), CON(HFD), CPS(LFD), and CPS(HFD)).

(legend continued on next page)

rhythms during pregnancy are conveyed to impact fetal counterparts and direct development and metabolic outcomes during adulthood in the offspring. Numerous endocrine and humoral factors have been implicated in mediation of maternal- and paternal-fetal circadian communication during pregnancy.[9,10] For instance, the offspring animals of mothers that undergo out-of-phase treatment with glucocorticoids later exhibit behavioral abnormalities such as increased anxiety and compromised stress tolerance.[11] Supporting this concept, the authors have previously revealed that short-chain fatty acids derived from the maternal gut microbiota impact organ development and differentiation in offspring.[12] Given the DOHaD theory, such maternal and/or paternal circadian fluctuations in humoral factors may play a pivotal role in dictating vulnerability to dietary habits in adulthood.[13]

To define the long-term effects of maternal circadian rhythms on metabolism in the progeny, we employed animal models of circadian rhythm disruption during pregnancy (CRD-P), including chronic phase shifting (CPS) of LD cycles and clock mutation. Despite reduced weight of the fetus and placenta of arrhythmic mothers, the offspring mice exhibited worsening of diet-induced obesity (DIO) in adulthood. Decreased energy expenditure and arrhythmic eating behavior underlay such exacerbation of obesity and were associated with the central leptin resistance in the offspring. Of interest, the manners in which hepatic circadian rhythms are reprogrammed by a high-fat diet (HFD) were altered by maternal CPS at the transcriptomic and metabolomic levels. Strikingly, chronic jetlag altered the circadian rhythms of the mother and fetus, leading to changes in the lag of phase between the mother and fetus. CRD-P caused a smaller placenta, although single-cell RNA sequencing (RNA-seq) revealed the induction of genes encoding lineage development, differentiation, and specificity in each placental cell type. Furthermore, time-restricted feeding (TRF) of the adult offspring failed to fully obliterate the additional weight gain elicited by maternal CPS in response to HFD, whereas the calorie-restricted (CR) food given every 24 h at the beginning of the night prevented such exacerbation of obesity. Collectively, these findings highlight that maternal circadian rhythms pertain to fetal development, such that dissonant rhythms *in utero* contribute to unremitting metabolic vulnerability in the adult progeny.

RESULTS

CPS of LD cycles during pregnancy impacts metabolic health of offspring

To investigate the impact of CRD-P on offspring, C57BL/6J pregnant mice were housed under a 12-h LD cycle (control [CON]) or CPS, a condition resembling a chronically jet-lagged state or a shift-working condition, immediately after a plug was confirmed (Figure 1A). In the CPS group, the LD cycle was phase-advanced by 8 h every 5 days, exclusively during pregnancy, as previously described.[14] Mice failed to become fully entrained within 5 days of a new LD cycle, leading to circadian perturbation (Figure 1B). Newborn animals from both groups were raised under normal LD conditions until the age of 4 weeks, when male offspring mice were subjected to *ad libitum* (AL) either HFD or low-fat diet (LFD) over 12 weeks (Figure 1A). Notably, the body weight of neonates born to CPS mothers was lower than those of neonates born to CON mothers (Figure 1C). Although this tendency persisted during LFD feeding, offspring from CPS mothers (hereafter "CPS offspring") developed marked obesity upon HFD feeding (Figures 1D, 1E, and S1A). The white adipose tissue (WAT) and liver weight of HFD-fed CPS offspring was higher than those of HFD-fed CON offspring at 16 weeks (Figures 1F and S1B). In line with the findings, maternal CPS led to remarkable histological alterations, such as lipid droplets in the liver, adipocyte expansion, and macrophage infiltration in WAT, under HFD conditions (Figures 1G, 1H, and S1C–S1G). By contrast, the body fluid levels did not differ between the groups (Figure S1H). Maternal CPS exposure elevated serum levels of total cholesterol (TC) and triglycerides (TGs) and impaired glucose tolerance and insulin sensitivity to a stronger degree on consumption of an HFD than the CON group (Figures 1I, 1J, and S1I). Metabolic cage analysis revealed that the HFD-induced reduction in oxygen consumption and energy

(B) Representative double-plotted actograms from the pregnant mice displaying 2 successive days for visualization. Dark phase is shadowed. Scale bar, 25 counts.
(C) BW of offspring (CON: $n = 6$; CPS: $n = 5$). $^{*}p < 0.05$ by two-way ANOVA (vs. CON).
(D) A representative image of the HFD-fed offspring.
(E) BW of offspring mice (CON(LFD): $n = 12–14$; CON(HFD): $n = 12–15$; CPS(LFD): $n = 10$; CPS(HFD): $n = 12$).
(F) Representative photograph (top) and weights ($n = 5–12$, bottom) of offspring tissues. epi, epididymal; peri, perirenal; sub, subcutaneous.
(G and H) Liver oil red O (G) and WAT F4/80 staining (H).
(I) Glucose (top) (CON(LFD): $n = 10$; CON(HFD): $n = 12$; CPS(LFD): $n = 7$; CPS(HFD): $n = 8$) and insulin (bottom) (CON(LFD): $n = 5$; CON(HFD): $n = 11$; CPS(LFD): $n = 9$; CPS(HFD): $n = 8$) tolerance tests.
(J) AUC of the glucose (top) and insulin (bottom) tolerance tests.
(K and L) Metabolic cage assessment of male offspring ($n = 7$).
(M and N) Daily food intake (M), adjusted by BW (N) ($n = 4$). L, light; D, dark.
(O) Gene expression in liver (top, $n = 3–6$) and WAT (bottom, $n = 4–5$).
(P) Protein expression in liver total lysates ($n = 3$ biological replicates).
(Q and R) Gene expression in liver (Q, $n = 3–6$) and WAT (R, $n = 4–5$).
(S) Serum leptin levels of HFD-fed offspring ($n = 4–5$).
(T) Gene expression in hypothalamus ($n = 4$).
(U) Protein expression in hypothalamus total lysates ($n = 3$ biological replicates).
(V) Serum leptin levels of 4-week-old offspring ($n = 4$).
(W and X) Daily food intake (W), adjusted by BW (X) of 4-week-old offspring ($n = 5$). L, light; D, dark. $^{*}p < 0.05$, $^{**}p < 0.01$, $^{***}p < 0.001$, and $^{****}p < 0.0001$ by two-way ANOVA (vs. CON(HFD)) (E, F, I–K, M, O, and Q–T). Data are presented as mean + SEM. ZT0 and ZT24 are double plotted for visualization (O and Q–T). See also Figure S1.

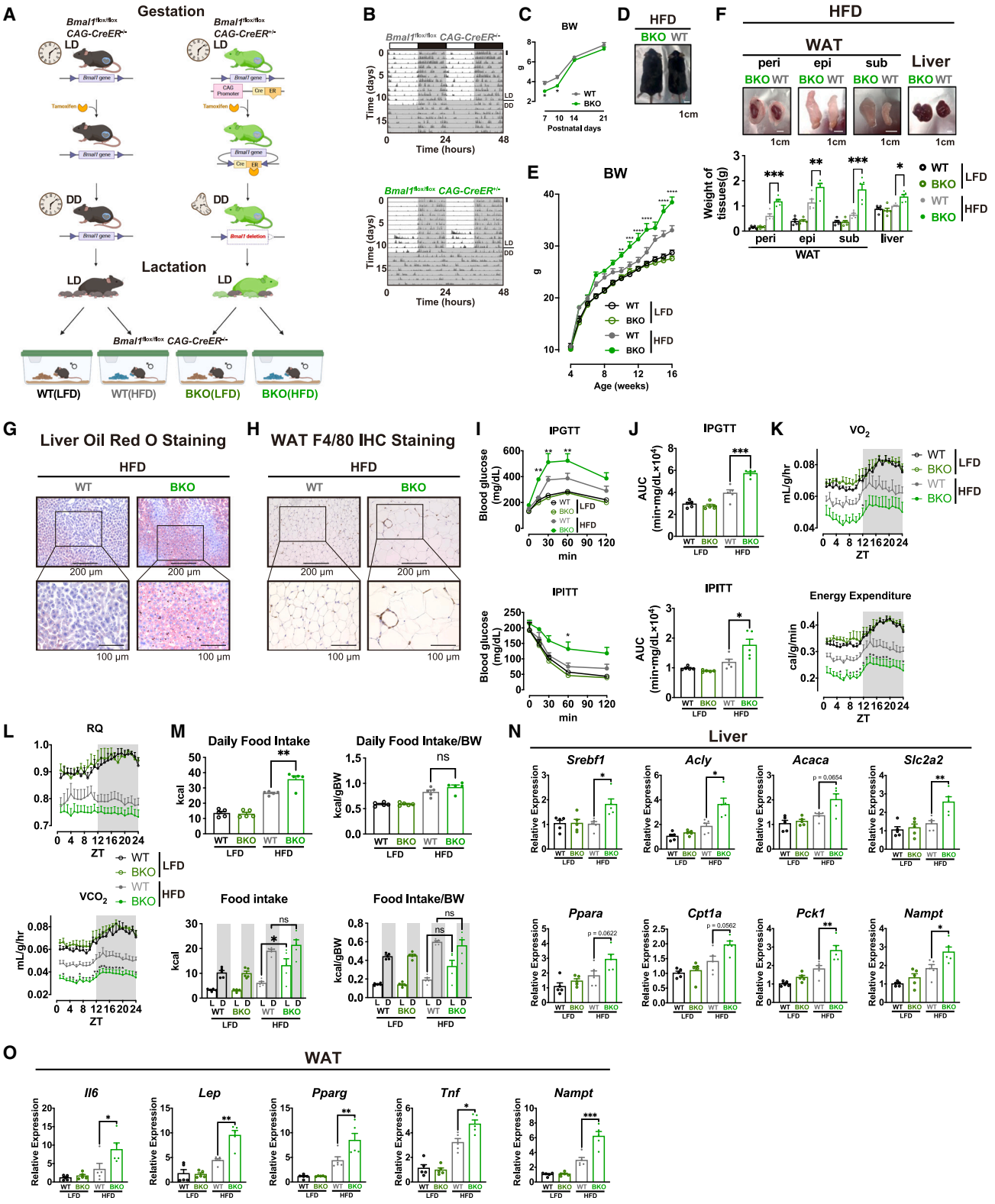

Figure 2. Offspring of *Bmal1*-deficient mothers display exacerbation of DIO

(A) Scheme for the inducible BKO following conception and WT offspring fed AL-HFD or LFD.

(B) Representative double-plotted actograms from pregnant mice displaying 2 successive days for visualization. Those pregnant mice were treated with tamoxifen from E7.5 to E11.5 and subsequently transferred to constant darkness. Scale bar, 25 counts.

(legend continued on next page)

expenditure was accelerated by maternal CPS exposure (Figures 1K and 1L). Daily food and water intake was increased as a result of maternal CPS, particularly during the light phase; however, the body-weight-adjusted daily food consumption was similar between the HFD-fed offspring groups (Figures 1M, 1N, and S1J). Such an increased food intake during the resting phase is associated with DIO as well as clock mutant models and potentially contributes to the increase in body weight and reduced energy expenditure.[15–18] The exacerbation of DIO and metabolic hallmarks of the HFD-fed male CPS offspring were also observed in the female offspring, albeit to a somewhat weaker degree (Figures S1K–S1R).

The free-running period of locomotor activity under constant darkness was virtually comparable between the HFD-fed offspring groups, suggesting that CRD-P had little effect on the intrinsic circadian period (Figures S1S and S1T). Similarly, gene and protein expression of the core clock machinery in the liver and WAT of HFD-fed offspring was minimally altered by maternal CPS, albeit with a tendency of slight phase advance and increased amplitude (Figures 1O, 1P, S1U, and S1V). On the other hand, the daily expression of genes related to fatty acid oxidation and lipogenesis in the HFD-fed CPS liver was more oscillatory, which is consistent with the previous observations of HFD-driven hepatic circadian reprogramming (Figures 1Q and S1U).[19,20] The expression of genes encoding adipokines and cytokines was upregulated, whereas that related to lipid oxidation was downregulated, by CPS in the WAT in response to HFD (Figure 1R). Of note, leptin is regulated by the circadian clock in adipose tissues; its dysfunction leads to increased food intake in the light phase and obesity, as observed in the HFD-fed CPS offspring.[21,22] The arrhythmicity of leptin gene expression was also observed at the serum level (Figure 1S). Despite the hyperleptinemia, however, expression of genes encoding orexigenic peptides, such as *Npy* and *Agrp*, was induced in the hypothalamus, particularly during the light phase, suggesting the central leptin resistance (Figure 1T). Consistently, phosphorylation of hypothalamic proteins in the leptin receptor signaling pathways was attenuated by maternal CPS (Figures 1U and S1W). In stark contrast, metabolic genes in the skeletal muscle and brown adipose tissue were virtually unaffected by maternal CPS (Figures S1X and S1Y). Of note, the increase in the serum leptin levels and food consumption of the HFD-fed CPS offspring in the light phase was absent at the beginning of HFD feeding (Figures 1V–1X). Overall, CPS during pregnancy disrupts diurnal feeding behavior and causes metabolic vulnerability to dietary challenges, thereby contributing to obesity in the offspring.

Genetic disruption of circadian rhythms during pregnancy recapitulates phenotype of offspring born to CPS mothers upon HFD challenge

To gain insight on whether the pronounced DIO phenotype elicited by maternal CPS is causally linked to maternal clock disruption, *Bmal1*$^{flox/flox}$ and CAG-CreER$^{+/-}$ mice were crossed to generate tamoxifen-inducible *Bmal1* knockout (BKO) mice. As such, the *Bmal1* gene was ablated systemically by tamoxifen following conception to circumvent infertility due to *Bmal1* deletion (Figure 2A). On embryonic day 7.5 (E7.5), pregnant mice were treated with tamoxifen via oral gavage for 5 days and then transferred to constant darkness to avoid photic entrainment (Figure 2A). Whereas *Bmal1*$^{flox/flox}$ CAG-CreER$^{-/-}$ (wild type [WT]) pregnant mice retained rhythmic locomotor activity, *Bmal1*$^{flox/flox}$ CAG-CreER$^{+/-}$ (BKO) pregnant mice failed to sustain such behavioral cycles under constant darkness following tamoxifen treatment, indicating the successful knockout of the *Bmal1* gene during pregnancy (Figure 2B). Indeed, the expression of *Bmal1* gene and protein as well as its transcriptional target, *Dbp*, was lost, whereas that of the reverse strand of ERBA (REV-ERBα) target genes, *Cry1* and *Npas2*, was derepressed in BKO mothers shortly after weaning (Figures S2A and S2B). Although body weight of the WT offspring born to BKO mothers (hereafter ''BKO mothers' offspring'') was lower than that of WT mothers' offspring during the early neonatal period, DIO effect on body weight was more striking in the BKO mothers' male offspring than in those from WT mothers from 10 weeks of age (Figures 2C–2E and S2C). Consistently, the tissue weight of WAT and liver was higher in BKO mothers' offspring on HFD (Figure 2F). Histological assessment revealed notable lipid accumulation in the liver and adipocyte hypertrophy accompanied by macrophage infiltration in WAT (Figures 2G, 2H, and S2D–S2H). Meanwhile, body fluid quantity was similar between the offspring mice of WT and BKO mothers (Figure S2I). Concomitantly, serum TC and TG concentrations were higher in BKO mothers' offspring, which was associated with HFD-induced glucose intolerance and insulin resistance (Figures 2I, 1J, and S2J). Metabolic cage analysis demonstrated that oxygen consumption and energy expenditure were diminished in the BKO mothers' offspring (Figures 2K and 2L). Food and water intake increased in the BKO mothers' offspring, albeit the body-weight-adjusted daily food consumption was comparable between the groups (Figures 2M and S2K). This worsening of DIO and metabolic signature of the HFD-fed, BKO mothers' male offspring were also observed in the female offspring (Figures S2L–S2S). The expression of hepatic genes encoding metabolic pathways such as fatty acid synthesis, oxidation,

(C) BW of offspring (WT: $n = 7$; BKO: $n = 5$–6). *$p < 0.05$ by two-way ANOVA (vs. WT).
(D) A representative image of the HFD-fed offspring.
(E) BW of the male offspring ($n = 5$).
(F) Representative photograph (top) and weights ($n = 5$, bottom) of tissues. epi, epididymal; peri, perirenal; sub, subcutaneous.
(G and H) Liver oil red O (G) and WAT F4/80 staining (H).
(I) Glucose (top) and insulin (bottom) tolerance tests ($n = 5$).
(J) AUC of glucose (top) and insulin (bottom) tolerance tests ($n = 5$).
(K and L) Metabolic cage assessment of male offspring mice ($n = 4$).
(M) Daily food intake (left) and food intake adjusted by BW (right) ($n = 5$). L, light; D, dark.
(N and O) Gene expression in liver (N) and WAT (O) ($n = 5$). *$p < 0.05$, **$p < 0.01$, ***$p < 0.001$, and ****$p < 0.0001$ by two-way ANOVA (vs. WT(HFD)). Data are presented as mean + SEM.
See also Figure S2.

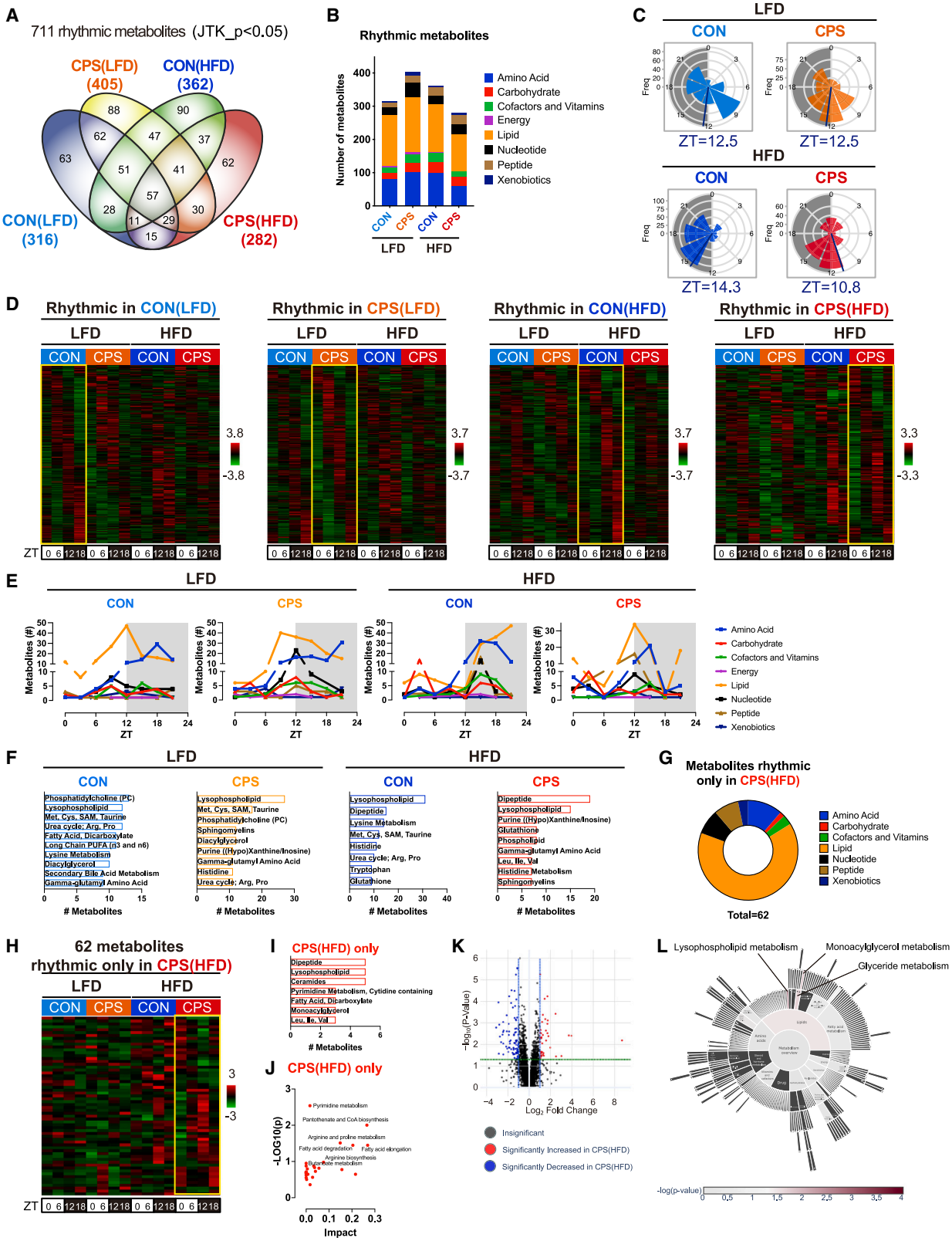

Figure 3. Hepatic metabolome reveals temporal rewiring of metabolic cycles by CRD-P

(A) Venn diagram showing the number of hepatic rhythmic metabolites in offspring (JTK_CYCLE, $p < 0.05$, $n = 5$ per time point per group).

(B) Numbers of rhythmic metabolites in each super-pathway.

(legend continued on next page)

and gluconeogenesis, along with those in WAT with regard to adipokines and cytokines, were upregulated in BKO mothers' offspring at zeitgeber time (ZT)12 (Figures 2N and 2O). By contrast, core clock genes were unaltered in BKO mothers' offspring (Figures S2T and S2U). Thus, offspring mice of clock-deficient mothers metabolically and phenotypically resembled those of CPS mothers in response to HFD, suggesting that the impact of CRD-P on long-term metabolic consequences is, at least partially, mediated by the circadian clock.

CRD-P rewires hepatic circadian reprograming by HFD

Nutritional challenges invoke temporal adaptive responses in a tissue-specific manner, leading to the remodeling of circadian rhythms in metabolism.[23–25] To clarify whether the *in utero* circadian environment influences the temporal response to dietary composition and metabolic trajectory after birth, a metabolomic analysis was implemented for liver samples using ultra-high-performance liquid chromatography-tandem mass spectroscopy (UPLC-MS/MS). In total, 981 annotated metabolites were identified (Table S1). Of all the metabolites, 711 metabolites were cyclic in at least one of the four groups of offspring mice, which was determined using Jonckheere-Terpstra-Kendall (JTK)-CYCLE analysis (Figure 3A). Whereas different classes of metabolites were oscillatory in each group, significant numbers of such metabolites were commonly rhythmic across the groups (Figures 3B, S3A, and S3B). The common cycling metabolites in all four groups exhibited similar phase distributions and amplitudes, and were overrepresented with amino acids and metabolites engaging in glycogen metabolism, whose robust diurnal variation has been well defined (Figures S3C–S3G).[26,27] The histogram and heatmap show distinct phase distribution in each group (Figures 3C and 3D). Specifically, HFD delayed and advanced the circadian phase in the CON and CPS offspring, respectively (Figure 3C). The breakdown of the histogram revealed each class of metabolites with various peak phases (Figure 3E). Furthermore, subclasses of oscillatory metabolites were enriched in each group (Figures 3F, S3E, S3F, and S3H).

To interrogate how CRD-P exacerbates obesity in an HFD-specific fashion, newly cyclic metabolites were examined in the HFD-fed CPS offspring. Of the 62 diurnal metabolites, nearly two-thirds were lipids (Figures 3G and 3H). Sub-pathway and enrichment analyses demonstrated that these oscillatory metabolites are comprised of lysophospholipids, ceramides, fatty acids, and monoacylglycerols (Figures 3I and 3J). Moreover, differentially expressed metabolites between the HFD-fed CON and CPS offspring were overrepresented with lipid species (Figures 3K, 3L, and S3I). Thus, maternal CPS resulted in the production of newly rhythmic lipid metabolites under HFD conditions. Overall, these results indicate that CRD-P reorganizes the temporal metabolic response to HFD in the liver.

Circadian reprogramming by HFD involves cyclic activation of the lipid regulators, sterol regulatory element-binding protein (SREBP) and peroxisome proliferator-activated receptors (PPARs), leading to *de novo* oscillations of hepatic genes.[19,20] Such circadian reprogramming was also suggested in the livers of HFD-fed CPS offspring in light of the rhythmic activation of genes involved in lipid metabolism (Figure 1Q). To delineate whether CRD-P alters circadian reprogramming by HFD, RNA-seq was undertaken for liver samples from the offspring (Table S2). Of the 24,883 annotated transcripts, 8,832 transcripts were cyclic in at least one of the four progeny groups (Figure 4A). A considerable number of transcripts were commonly rhythmic across the different groups (Figures 4A and S4A). Common oscillatory transcripts in all four groups exhibited comparable phase and amplitude distributions between CON and CPS groups, and were enriched with core clock components, reflecting the resilience of the circadian clock (Figures S4B–S4E). In contrast, phase distribution of the oscillatory genes differed in each group (Figure 4B). Dietary fat and CRD-P drove divergent daily pathways in the liver (Figures 4C, 4D, and S4D). In an attempt to further clarify which diurnal metabolic pathways were coherent in the metabolome and transcriptome, integrative joint pathway analysis was employed.[28] Distinct pathways were overrepresented in each group of mice (Figure 4E).

Maternal CPS evoked a considerable number of newly cyclic transcripts in the liver in an HFD-specific manner (Figure 4F). These 1,029 genes were enriched with long-chain fatty acid metabolic processes and regulation of nuclear factor κB (NF-κB) signaling pathways, which is in line with the worsening of HFD-induced fatty liver because of CRD-P (Figure 4G). Consistently, upregulated genes in the HFD-fed CPS offspring in comparison with the CON offspring were enriched with lipid metabolic processes (Figures S4F and S4G). Joint pathway analysis also revealed the highest enrichment of fatty acid elongation in the HFD-fed CPS offspring (Figures 4H and 4I).

To examine whether CRD-P reshapes the gut diurnal microbiome, 16S rRNA sequencing was performed in the CPS offspring at ZT0 and ZT12 (Table S3). Principal-component analysis revealed that the dietary (LFD vs. HFD) and diurnal (day vs. night) effects resulted in distinct profiles of the gut microbiome, as reported previously (Figure S4H).[29,30] In comparison with these differences, the overlap between the maternal circadian rhythms (CON vs. CPS) was substantially larger, indicating that the impact of CRD-P on the gut microbial community is minimal (Figure S4H). Likewise, the proportion and diversity of the gut microbial species appeared to be influenced primarily by diet types and circadian effects but not by gestational chronodisruption

(C) Polar histograms showing the peak phase distribution of rhythmic metabolites.
(D) Heatmaps illustrating diurnal metabolites.
(E) Histogram indicating the peak phase of rhythmic metabolites in individual super-pathways.
(F) Sub-pathway analysis on diurnal metabolites.
(G) Pie chart illustrating the numbers of super-pathway metabolites rhythmic exclusively in CPS(HFD).
(H) Heatmap illustrating diurnal metabolites oscillating exclusively in CPS(HFD) condition.
(I and J) Sub-pathway (I) and pathway (J) analysis on diurnal metabolites rhythmic exclusively in CPS(HFD) condition.
(K) Volcano plot showing differentially expressed metabolites in the liver of the HFD-fed CPS offspring (vs. CON). $p < 0.05$.
(L) Representative sunburst visualization of the hepatic pathway enrichment comparing the HFD-fed CON and CPS offspring at ZT0.
See also Figure S3 and Table S1.

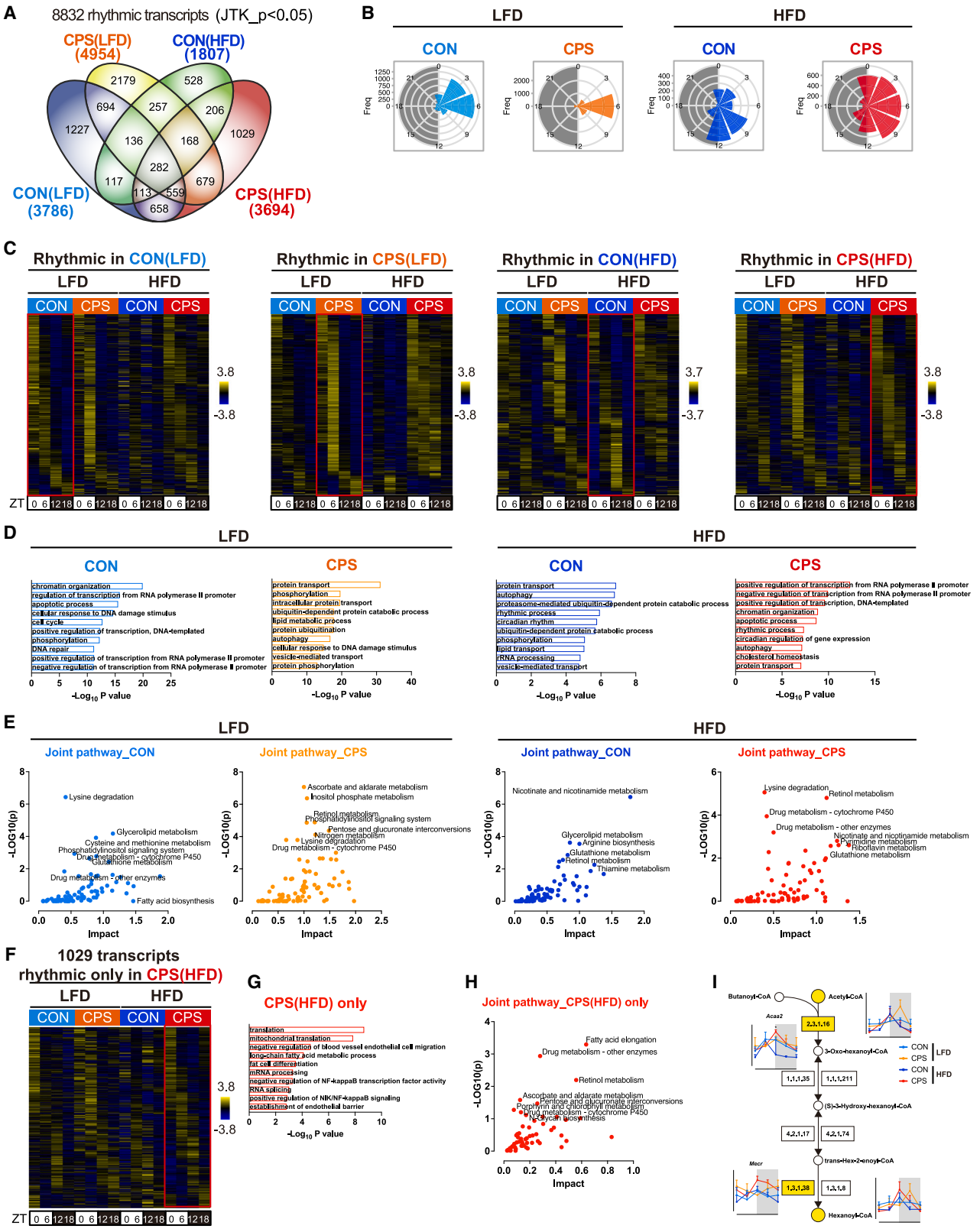

Figure 4. CRD-P modulates hepatic circadian reprogramming by HFD

(A) Venn diagram showing the number of hepatic rhythmic transcripts in offspring (JTK_CYCLE, $p < 0.05$, $n = 3$ per time point per group).

(B) Polar histograms showing the peak phase distribution of rhythmic transcripts.

(legend continued on next page)

(Figures S4I–S4L). Overall, CRD-P reshaped the hepatic circadian reprogramming by HFD in light of increased lipid accumulation in the liver, thus inducing *de novo* oscillation in lipid metabolism.

CRD-P alters the phase-relationship of hepatic circadian rhythms between mother and fetus

The master pacemaker in the SCN synchronizes peripheral clocks in all the other tissues. We reasoned that the mammalian fetal circadian system could largely rely on that in pregnant mothers.[31] Hence, we investigated whether circadian rhythms of the maternal and fetal livers are temporally orchestrated during fetal development and whether such coordination, if present, is perturbed by CRD-P. The daily food and water consumption was virtually unchanged by CRD-P during late gestation, with an increased trend of food intake in BKO mothers (Figures S5A and S5B). Oscillatory expression of the circadian clock gradually emerges and becomes discernible during late gestation.[32,33] Hence, maternal and fetal tissues were collected on E18.5. First and foremost, the pregnancy duration of CPS and BKO mothers was slightly, but significantly, shorter than that of CON and WT mothers (Figure 5A). While the number of fetuses per mother was comparable, there was a tendency for reduced body and liver weight in fetuses from the CPS and BKO mothers, which is consistent with the reduced body weight of newborns from those mothers (Figures 1C, 2C, 5B, 5C, S5C, and S5D). Conversely, expression of genes associated with hepatocyte lineage and specificity was comparable in the fetal CON and CPS liver (Figure S5E). CPS caused 2 to 10 h of delay in the peak phases of the maternal core clock components, reaffirming that the clock was being re-entrained by shift in the LD cycles (Figures 5D and S5F). Notably, a recognizable degree of oscillation in gene expression was detected in the fetal liver clocks (Figures 5E and S5G). Importantly, hepatic clock gene expression was virtually in phase between the mother and fetus under the CON condition (Figures 5D, 5E, S5F, S5G). By contrast, a somewhat altered phase-relationship was appreciated by CPS in some clock genes (Figures 5D, 5E, S5F, and S5G). These findings implied that CRD-P may uncouple maternal clocks from fetal clocks, leading to the altered phase-relationship of circadian rhythms between mother and fetus. Supporting the phenomenon, serum levels of corticosterone, a synchronizer of peripheral clocks, were dampened and phase-delayed by CPS (Figure 5F).

These findings raised the possibility that maternal-fetal circadian synchronization plays a vital role in fetal development. To broaden the view of the maternal-fetal circadian resonance, RNA-seq was conducted (Table S4). As expected, CPS diminished the number of oscillatory transcripts dramatically (Figures 5G and 5H) and delayed their phase in mothers (Figure 5I), albeit with comparable amplitudes (Figure 5J). Strikingly, maternal CPS increased the number of rhythmic genes (Figures 5K and 5L) and advanced their phase in fetal livers (Figures 5M and 5N). Notably, annotations related to immunity and inflammation were overrepresented in the CPS liver in mother and fetus (Figures 5O and 5P). Commonly cyclic transcripts between the mother and fetus were confined (Figures 5Q–5T), and their maternal-fetal phase lag was similarly distributed in both CON and CPS conditions (Figure 5U).

Environmental factors at early life stages are implicated in invoking epigenetic changes and impacting susceptibility to obesity in later life.[34] To test whether CRD-P evokes altered DNA methylation, reduced representation bisulfite sequencing was conducted using the liver of fetus and 4-week-old mice from the CPS mothers. The methylation level at common CpG sites was highly correlated between any two samples (Figure S5H). Clustering showed that the CpG methylation of CPS fetal liver was more akin to that of CON fetal liver than to that of CPS offspring mouse liver, indicating that the developmental effect is more predominant than CRD-P in dictating the epigenetic landscape of DNA methylation (Figure S5I). In support of the observation, 3 weeks of maternal CPS before pregnancy (CPS-BP) did not influence the pregnancy period or fetal size as in the case of maternal CPS during pregnancy (Figures S5J–S5M). Thus, hepatic epigenetic changes did not seem to be involved primarily in the obese phenotype of progeny.

Considering the fact that *Bmal1* deletion was induced at E7.5, it could be hypothesized that the latter two-thirds of the gestational period may be sufficient and critical when the CPS exerts its effect on the fetus. However, CPS during the latter two-thirds of pregnancy (2/3CPS) failed to reproduce the shortened gestational period and reduced fetal weight as noted in CPS throughout the pregnancy and the BKO pregnant mice (Figures S5N–S5Q). Under the CPS condition, the maternal peripheral clock expression was phase-delayed in the process of re-entrainment to a new cycle yet retained rhythmicity in the liver, as observed previously (Figures 5D and S5F).[35] Conversely, *Bmal1* was deleted in all the maternal tissues of BKO mice (Figures S2A and S2B). Such a difference may explain why 2/3CPS did not generate similar effects as BKO, in spite of the same period of CRD-P. Nevertheless, the BKO animal model is considered informative, as it caused the phenotypic features in the offspring resembling the CPS progeny.

CRD-P reshapes the genomic signature of the placenta

During pregnancy, the placenta functions as an environmental interface between the mother and fetus to engage in the transport of essential nutrients, waste products, and gas exchange, thus

(C) Heatmaps illustrating diurnal transcripts.
(D) GO terms of biological processes enriched in cyclic genes.
(E) Joint pathway analysis of cyclic metabolites and transcripts.
(F) Heatmap illustrating diurnal transcripts oscillating exclusively in CPS(HFD) condition.
(G) GO terms of biological processes enriched in genes cycling exclusively in CPS(HFD) condition.
(H) Joint pathway analysis of metabolites and transcripts cyclic exclusively in CPS(HFD) condition.
(I) Example of the pathways jointly rhythmic exclusively in CPS(HFD) condition. The diagram represents a part of fatty acid elongation (KEGG). Metabolites, circles; genes, rectangles. EC number is given for specific enzymatic activity. Data are presented as mean + SEM. ZT0 and ZT24 are double plotted for visualization. *$p < 0.05$ by two-way ANOVA (vs. WT(HFD)).
See also Figure S4 and Table S2.

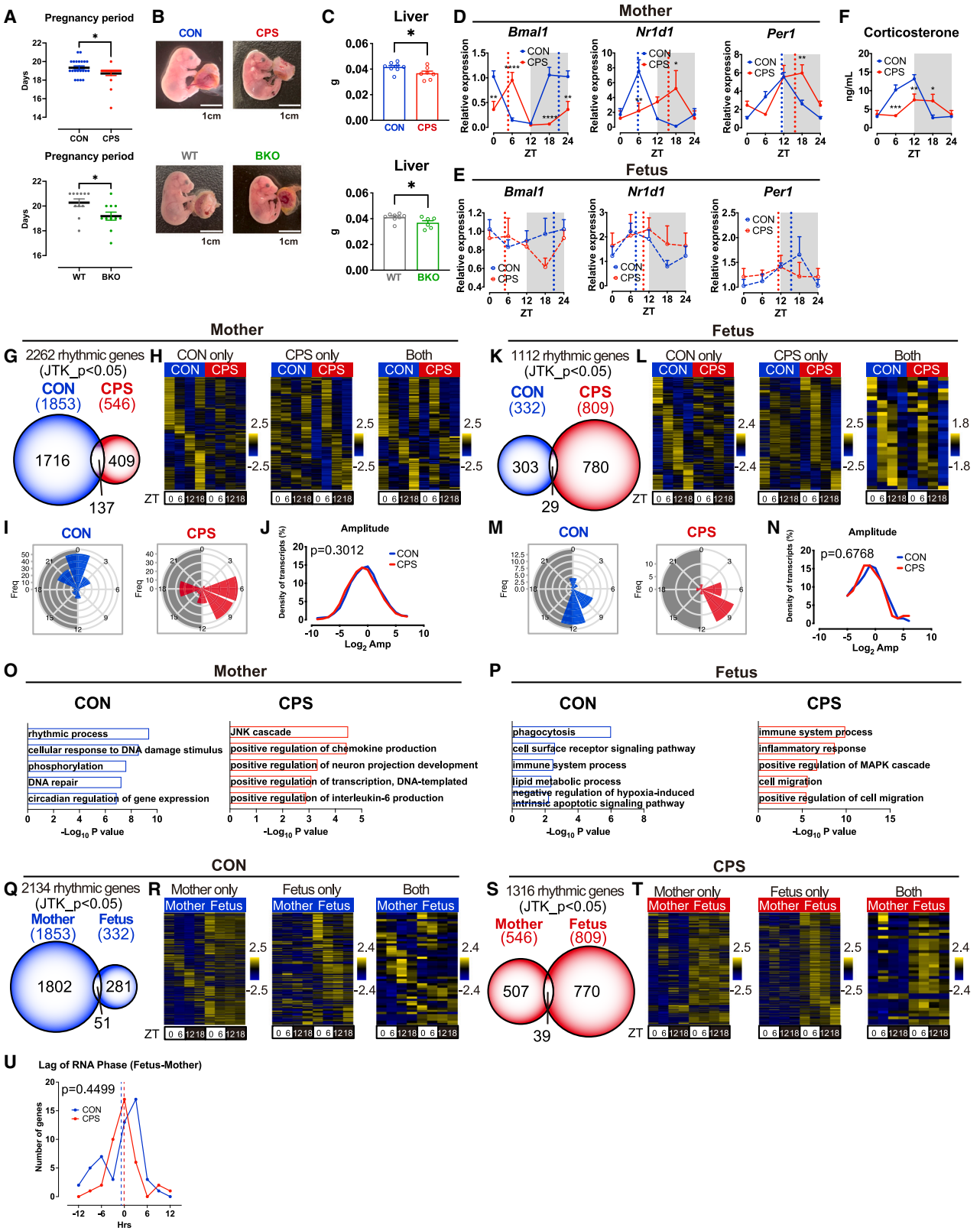

Figure 5. CRD-P influences rhythmic gene expression in fetal liver

(A) Pregnancy duration of CON and CPS mothers (top, *n* = 21) and of WT and BKO mothers (bottom, *n* = 11).

(B) Representative images of fetuses on E18.5.

(legend continued on next page)

ensuring normal fetal growth.[36,37] Maternal undernutrition may compromise feto-placental growth, resulting in an adaptive, smaller placenta, with an increase in fetal to placental weight ratio in an effort to improve efficiency in nutritional transport.[38] As such, the placenta may convey temporal signals and bridge the maternal and fetal circadian systems. Hence, we investigated whether CRD-P influences placental development and genomic profiles. In line with the reduced body weight of fetuses and neonates, placental weight was decreased in CPS and BKO mothers (Figure 6A). Histological evaluation also demonstrated a slightly smaller placenta with a virtually intact labyrinth structure in CPS and BKO mothers (Figure 6B). In contrast, expression of placental marker genes or those encoding chorioallantoic branching, labyrinthine development, and glucose and amino acid transporters was upregulated by maternal CPS (Figures 6C, 6D, and S6A). Expression of the core clock genes was also induced by CPS (Figures 6D and S6A). In support of this observation, the fetal body weight to placental weight ratio was higher in CPS and BKO mothers than those in CON and WT mothers, indicating that CRD-P enhances placental efficiency (Figure 6E). Notably, neither maternal CPS prior to pregnancy nor during the latter two-thirds of pregnancy resulted in any changes in placental weight or the fetal body weight to placental weight ratio (Figures S6B–S6E).

To dissect whether CRD-P impacts the placental genomic signature, RNA-seq at single-nuclei resolution was performed on account of the heterogeneous cellular populations and developmental states that constitute the placenta. A uniform manifold approximation and projection (UMAP) plot identified 14 distinct clusters based on the expression profiles (Figures 6F–6H and S6F–S6H); among them, the 12 clusters could be annotated: (Figures 6I and S6I).[39] While the proportion of decidual stroma (cluster 3) was reduced, those of endothelial (cluster 8) and blood and immune cells (cluster 11) were increased by maternal CPS (Figure S6F). In each cluster, the distinct Gene Ontology (GO) terms were noted in upregulated and downregulated genes, respectively (Figure S6J).

In line with the upregulation of placenta-specific marker genes (Figure 6C), those encoding trophoblast lineage development, cell differentiation, chorioallantoic branching and labyrinthine development, nutrient transport across labyrinth, trophoblast stem cell niche, trophoblast-specific genes, and core clock genes, tended to be upregulated in the CPS placenta (Figure 6I). Crucially, the *Prl2c2* gene, encoding the endocrine hormone Proliferin-1, which is implicated in embryonic development, was repressed in CPS trophoblast glycogen cells (cluster 0) (Figure 6I). Genes were expressed differentially following maternal CPS in spatially segregated placental regions (Figure 6J). Interestingly, the GO term "*in utero* embryonic development" was enriched in downregulated genes in all regions, whereas "female pregnancy" was the most overrepresented term in the decidua and junction (Figure 6K). Collectively, these results suggest that CRD-P affects placental gene regulation, such that it expedites placental efficiency and minimally influences fetal growth.

Circadian alignment of CR, not TRF alone, ameliorates the worsened DIO in offspring as a result of CRD-P

The arrhythmic eating behavior with increased food intake during the light phase underlies the worsened DIO in the offspring experiencing CRD-P. To test whether reinstating circadian rhythms in adulthood abrogates such DIO exacerbation caused by CRD-P, the offspring mice were subjected to an HFD under TRF (HFD_TRF) exclusively during the dark phase over 12 weeks, and the findings were compared with those of the AL-fed cohorts of mice described in Figure 1 (Figure 7A). TRF prevented body weight gain in the offspring mice in both maternal circadian photic conditions compared with their AL-fed counterparts (Figure 7B). However, a significant degree of obesity remained following TRF in the CPS offspring from 14 weeks of age, albeit with the body fluid levels and water intake similar to the CON offspring (Figures 7B and S7A–S7D). This manifestation of HFD_TRF is also reflected by the tendency of higher WAT and liver weights in the CPS offspring than those in the CON offspring (Figure 7C). In parallel, hepatic lipid droplets and adipocyte hypertrophy in the CPS offspring were not as improved as those in the CON offspring upon HFD_TRF (Figures 7D, 7E, and S7E). In support of this phenotypic difference, serum lipid profiles, glucose tolerance, and insulin sensitivity in the CPS offspring were not restored to the same extent as those in the CON offspring following HFD_TRF (Figures 7F, 7G, and S7F). Consistently, metabolic cage analysis showed an increase in respiratory quotient, oxygen consumption, and energy expenditure in the TRF regimen, though lower in the CPS offspring than CON offspring (Figure 7H). Importantly, daily food consumption was similar between the TRF groups, albeit with an increased consumption trend in the TRF-subjected CPS offspring (Figure 7I).

(C) Liver weight on E18.5 (n = 6–8).
(D and E) Gene expression in maternal (D) and fetal livers (E). Dotted lines indicate peak phases determined by Cosinor analysis (n = 3–5).
(F) Serum corticosterone levels of mothers (n = 4).
(G and K) Venn diagram showing the number of rhythmic transcripts in maternal (G) and fetal livers (K) (JTK_CYCLE p<0.05, n=3 per time point per group).
(H and L) Heatmaps illustrating maternal (H) and fetal (L) hepatic diurnal transcripts oscillating only in CON (left), CPS (middle), and both (right).
(I and M) Polar histograms showing the peak phase distribution of maternal (I) and fetal (M) hepatic transcripts commonly rhythmic in CON and CPS conditions.
(J and N) Distribution of amplitude in maternal (J) and fetal (N) hepatic transcripts commonly oscillating in CON and CPS conditions.
(O and P) GO terms of biological processes enriched in maternal (O) and fetal (P) hepatic cyclic genes.
(Q and S) Venn diagram showing the number of hepatic rhythmic transcripts in CON (Q) and CPS (S) conditions (JTK_CYCLE $p < 0.05$, $n = 3$ per time point per group).
(R and T) Heatmaps illustrating hepatic diurnal transcripts oscillating only in mothers (left), fetus (middle), and in both (right) in CON (R) and CPS (T) conditions.
(U) Distribution of hepatic peak phase lags of fetus compared with mother.
Data are presented as mean ± SEM (A) and mean + SEM (C–F). ZT0 and ZT24 are double plotted for visualization (D–F). $^{*}p < 0.05$, $^{**}p < 0.01$, $^{***}p < 0.001$, and $^{****}p < 0.0001$ by Student's t test (A and C) or by two-way ANOVA (vs. CON; D and F).
See also Figure S5 and Table S4.

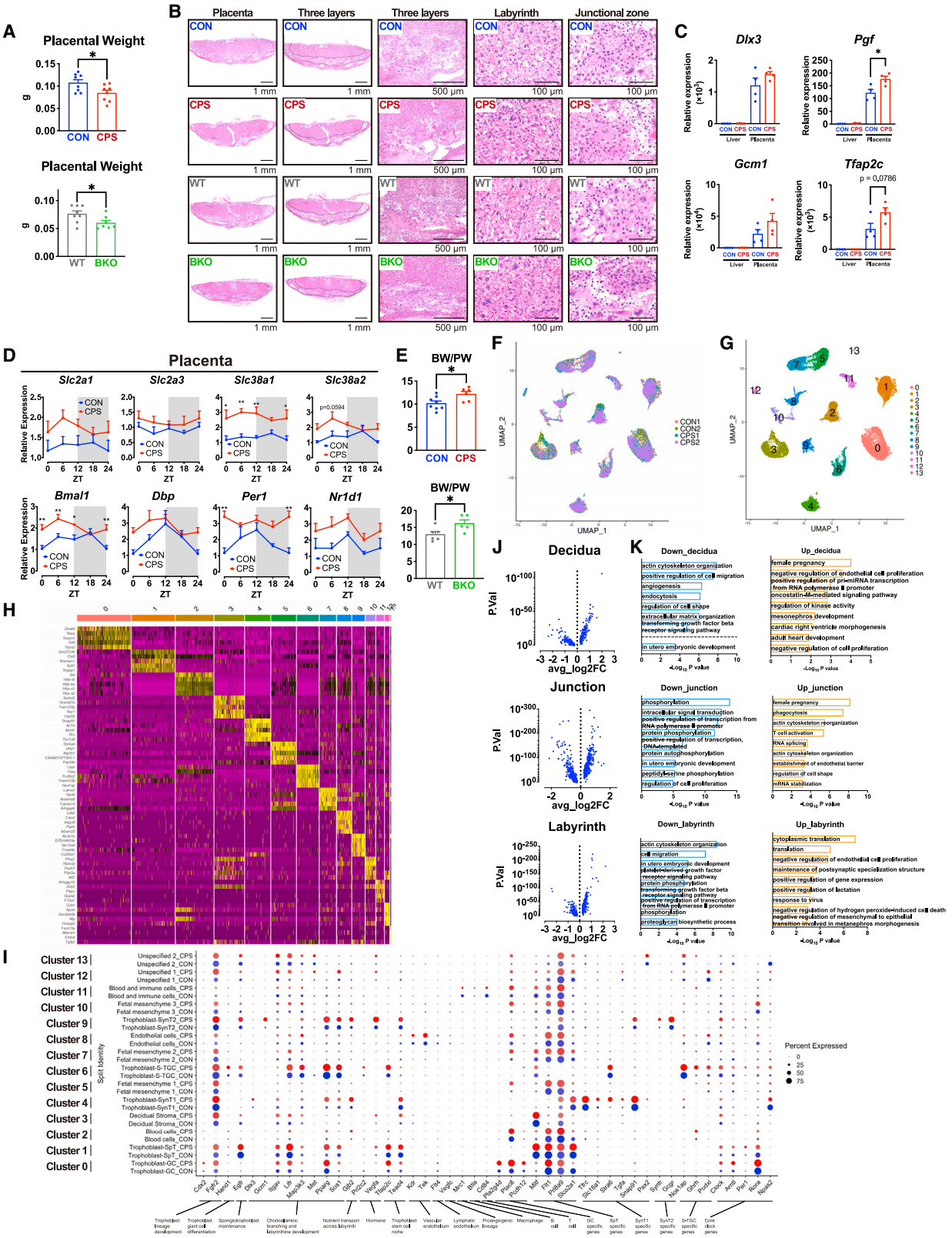

Figure 6. CRD-P impacts placental genomic signature

(A) Placental weight in CON and CPS conditions (n = 8, top) and in WT and BKO mice (WT: n = 8; BKO: n = 7, bottom) on E18.5.

(B) H&E staining of placenta. Three layers of placenta are indicated by black lines; top, labyrinth; middle, junctional zone; bottom, decidua.

(legend continued on next page)

The TRF regimen drives circadian rhythms by controlling metabolic regulators and restoring the amplitude of circadian oscillators in the liver.[40] The hepatic transcript levels of *Bmal1, Cry1*, and *Nampt* were equally restored in both TRF groups (Figures 7J and S7G). Importantly, oscillatory expression of *Nr1d1*, *Dbp*, *Per1*, *Per2, Slc2a2*, and *Pck1* in the CPS offspring did not recover to the same extent as that in CON offspring following HFD_TRF, which is consistent with the metabolic features (Figures 7J and S7G). On the contrary, differences in gene expression of core clock components as well as the cytokines and adipokines in the WAT of TRF-subjected CON and CPS offspring was minimal (Figures S7H and S7I).

To ascertain whether the increased food consumption trend in the TRF-subjected CPS offspring contributes to the persisting obesity, CR, in alignment with the onset of the active phase, was implemented, in which male offspring mice received an identical amount of HFD supplied every 24 h at ZT12 (HFD_CR) over 12 weeks (Figure 7K). Under the CR condition with daily food replenishment, mice self-impose TRF.[41] Hence, HFD_CR can be considered a type of dietary intervention where CR is added to TRF. HFD_CR reduced the body weight gain of CPS offspring to the same degree of CON offspring (Figures 7L and 7M). The WAT and liver weights were comparable between the HFD_CR-fed CON and CPS offspring (Figure 7N). In agreement with these observations, glucose tolerance, insulin sensitivity, oxygen consumption, and energy expenditure (Figures 7O–7Q), along with daily food and water consumption and body fluid levels, were similar between the groups (Figures 7R–7T). These metabolic features of the HFD_CR-fed male offspring were also observed in female offspring mice (Figures S7J–S7S). Collectively, the combination of CR and TRF, but not TRF alone, fully counteracts the DIO exacerbation in offspring because of CRD-P. Overall, CRD-P results in the arrhythmic eating behavior with increased food consumption, reduced energy expenditure, and aggravation of DIO and fatty liver that are associated with the rewiring of hepatic circadian reprograming, thereby dictating metabolic plasticity in the offspring.

DISCUSSION

Temporal communication is the key to advancing our understanding of how tissue-level rhythmicity is orchestrated across distal organs and relies on circadian networks.[27,42,43] Because the *in utero* environment is influenced by maternal metabolic and nutritional states, and is considered a major external input for the fetus, it could be postulated that circadian maternal-fetal communication is established during pregnancy and plays far-reaching roles in development at early life stages and metabolic outcomes in offspring. In other words, maternal circadian rhythms may somehow be conveyed to the fetus such that synchrony between the mother and fetus expedites organ maturation, thereby imparting metabolic resilience to aberrant dietary habits. In the present study, we profiled DIO exacerbated by CRD-P using CPS and BKO animals and uncovered that a combination of increased and arrhythmic food intake, reduced oxygen consumption and energy expenditure, insulin and leptin resistance, and worsening of adipose tissue inflammation underlies the obesity and fatty liver phenotype. To our surprise, this obesity phenotype was not fully prevented by TRF alone but by a combination of CR and TRF of HFD, suggesting that metabolic programming during early life stages may dictate the rhythm of feeding behavior in later life. Further studies are required to decipher the molecular mechanisms by which CRD-P contributes to the altered feeding behavior in offspring.

The circadian clock does not operate in pluripotent stem cells (PSCs), but it starts to oscillate during differentiation, hence endogenous circadian rhythms gradually arise and amplify at the tissue level during the fetal and neonatal stages.[33,44] This fundamental biochemical event is most likely linked to ontogenesis, differentiation, proliferative metabolism, and functional maturation. Indeed, we observed that cellular reprogramming from somatic cells to PSCs seems to be coupled with cessation of the molecular clockwork and metabolic shifting to lipid synthesis.[45] Remarkably, periodic media changes in PSCs promote beta-cell differentiation, which is presumably explained by the entrainment of cell-autonomous circadian clocks leading to mature glucose responsiveness.[46] Conversely, the absence of *Bmal1* during development adversely impacts lifespan and relates to an aging-like phenotype, based on the fact that inducible BKO as late as 3 months of age produces little abnormality, which is appreciated in conventional BKO mice.[47,48] Interestingly, maternal and fetal circadian rhythms during pregnancy are almost in phase and entrainable by timed food intake of the mother.[49] Therefore, it could be inferred that periodic cues from the mother may help establish circadian rhythms and organogenesis in the offspring.[50,51] Contrary to our expectations, however, expression of genes encoding hepatocyte lineage markers was unaltered by maternal CPS. Additionally, organ development and structure appeared grossly intact, although fetal size and neonatal body weight were reduced by CRD-P. Hence, CRD-P may impinge on the metabolic programs of the offspring, at least partly independent of organ differentiation or maturation.

In conclusion, our study highlights that metabolic susceptibility to dietary stress is subject to the circadian environment at an early stage of life. Deciphering the temporal landscape of the endocrine and metabolic codes that are reciprocally communicated between the mother and fetus provides holistic views on

(C) Expression of placental marker genes (n = 4).
(D) Gene expression in placenta (n = 4–5). ZT0 and ZT24 are double plotted for visualization.
(E) Ratio of fetal body to placental weight (CON: n = 8; CPS: n = 6, top), (WT: n = 6; BKO: n = 5, bottom) on E18.5.
(F and G) UMAP visualization of placental cells colored by different samples (F) and cell types (G).
(H) Heatmap illustrating differentially expressed genes. Yellow and purple indicate high and low expression, respectively.
(I) Dot plots showing differential expression profiles across clusters (dot size) and groups (dot color). SynT, syncytiotrophoblast; S-TGC, sinusoidal trophoblast giant cells; SpT, spongiotrophoblast; GC, glycogen cells.
(J) Volcano plots showing differentially expressed genes.
(K) GO terms of biological processes. Data are presented as mean + SEM. *$p < 0.05$ and **$p < 0.01$ by Student's t test (A, C, and E) or by two-way ANOVA (D). See also Figure S6.

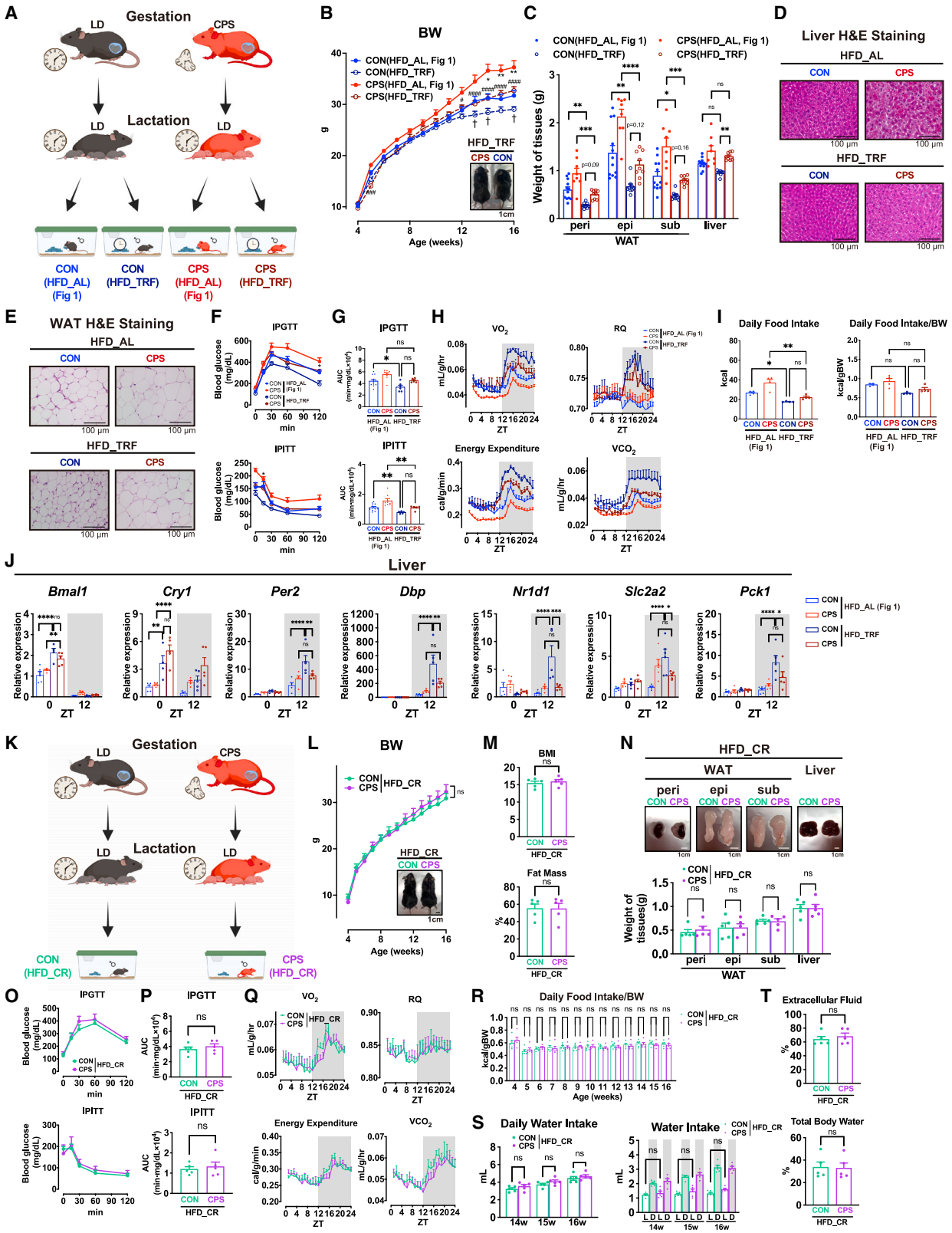

Figure 7. Circadian alignment of CR, not TRF alone, abolishes DIO phenotype of offspring caused by CRD-P

(A) Scheme for CPS during pregnancy and offspring mice placed on time-restricted access to HFD, which was compared with the AL-HFD feeding cohort in Figure 1.

(legend continued on next page)

how a staggering number of environmental factors are integrated optimally to promote resilience. Multidisciplinary support for maternal circadian rhythms may help navigate preventive strategies to expedite fitness in subsequent generations.

Limitations of the study

The impact of CRD-P on maternal nursing behaviors, including breastfeeding, was not assessed. Delayed weaning in rats prevents the animals from DIO later in life via the hypothalamic action of fibroblast growth factor 21 (FGF21).[52] Hence, the effect of CRD-P observed in this study may be partially attributable to potential alterations in maternal nursing behaviors during lactation. In addition, we could not fully distinguish whether the arrhythmic eating behavior and leptin resistance are the cause or effect of the exacerbated obesity due to maternal CPS. We cannot exclude the possibility that the differences in body weights between the HFD-fed CON and CPS offspring influenced the hepatic transcriptome and metabolome. Besides leptin, gut-derived hormones such as glucagon-like peptide-1 (GLP-1) and peptide YY (PYY) may also influence host appetite. Similarly, epigenetic mechanisms may be involved in the extrahepatic tissues of the CPS offspring, as the DNA methylation was assessed only in the liver.

RESOURCE AVAILABILITY

Lead contact

Further information and requests for resources and reagents should be directed to and will be fulfilled by the lead contact, Kenichiro Kinouchi (kenk@keio.jp).

Materials availability

This study did not generate new unique reagents.

Data and code availability

The accession number for the RNA-seq data reported in this study is GEO: GSE236201; single-cell RNA-seq data, GEO: GSE235916; 16S rRNA gene amplicon sequencing analysis, PRJNA1096943; and reduced representation bisulfite sequencing data, GEO: GSE263993. The uncropped, high-resolution scans of the western blots and values that were used to generate the graphs in this paper are presented in Data S1—source data. Any additional information required to reanalyze the data reported in this paper is available from the lead contact upon request. This paper does not report original code.

ACKNOWLEDGMENTS

We thank all members of the Itoh and Hayashi Laboratory for their inspiring discussions and technical assistance. We also thank Melanie Oakes, Seung-Ah Chung, and Yuzo Kanomata from the Genomics High-Throughput Facility at the University of California, Irvine; Kenji F Tanaka from the Division of Brain Sciences, Institute for Advanced Medical Research, Keio University School of Medicine; Isao Kurihara from the National Defense Medical College; Kazutoshi Miyashita, Sakiko Kobayashi, and Ayano Takeda from the Keio University School of Medicine; and Reiko Nakanishi from the Graduate School of Medicine at the University of Tokyo. K. Kinouchi was funded by JSPS KAKENHI (19K09012), The Japan Diabetes Society, and the Astellas Foundation for Research on Metabolic Disorders. K. Kinouchi, J.I., and H.I. received funding from JSPS KAKENHI(21K18270). H.I. was funded by the Japan Endocrine Society. S.N. was funded by the Japan Agency for Medical Research and Development (JP22ama121016). The work of K.C.A., S.A., and P.B. is in part supported by grant NIH R01GM123558 to P.B. Y.M. was supported by JSPS KAKENHI (24H00633 and 24K22126) and the Japan Science and Technology Agency FOREST (JPMJFR235H). A.S. was funded by JSPS KAKENHI (23H03848 and 23K24805). We would like to thank Editage (www.editage.jp) for English language editing. The graphical abstract and schemes in the figures were created in BioRender. Kinouchi, K. (2023) https://BioRender.com/q70h281.

AUTHOR CONTRIBUTIONS

Conceptualization, N.Y., K. Kinouchi, and H.I.; methodology, S.K., J.K., A. Itoh, S. Yamaguchi, H.H., S. Yuasa, A.S., Y.M., S.U., T.U., and S.N.; formal analysis, N.Y., K. Kinouchi, M.K., K.C.A., S.A., S.N., P.B., and H.I.; investigation, N.Y., K. Kinouchi, M.K., H.M., T.T., T.K., A. Iwahara, and S.K.; data curation, K. Kinouchi, M.K., K.C.A., S.A., Y.M., and P.B.; writing – original draft, N.Y., K. Kinouchi, and H.I.; writing – review & editing, K. Kato, S.T., T.N., J.Y., J.I., and K.H.; funding acquisition, K. Kinouchi, J.I., S.N., and H.I.

DECLARATION OF INTERESTS

The authors declare no competing interests.

(B) BW of offspring (n = 10–12). A representative image of the time-restricted, HFD-fed offspring. $^{\dagger}p < 0.05$, $^{\#}p < 0.05$, $^{\#\#\#}p < 0.001$, $^{\#\#\#\#}p < 0.0001$, $^{*}p < 0.05$, and $^{**}p < 0.01$ by two-way ANOVA (†: CON(HFD_AL) vs. CON(HFD_TRF); $^{\#}$: CPS(HFD_AL) vs. CPS(HFD_TRF); *: CON(HFD_TRF) vs. CPS(HFD_TRF)).
(C) Tissue weights (CON(HFD_AL): n = 12; CON(HFD_TRF): n = 8–9; CPS(HFD_AL): n = 8; CPS(HFD_TRF): n = 8–9). epi, epididymal; peri, perirenal; sub, subcutaneous.
(D and E) H&E staining of liver (D) and WAT (E).
(F) Glucose (top, CON(HFD_AL): n = 12, CPS(HFD_AL): n = 8, CON(HFD_TRF): n = 6, CPS(HFD_TRF): n = 6) and insulin (bottom, CON(HFD_AL): n = 11, CPS(HFD_AL): n = 8, CON(HFD_TRF): n = 5, CPS(HFD_TRF): n = 5) tolerance test. $^{*}p < 0.05$ by two-way ANOVA (CON(HFD_TRF) vs. CPS(HFD_TRF)).
(G) AUC of glucose (top) and insulin (bottom) tolerance test.
(H) Metabolic cage assessment of male offspring (AL groups: n = 7; TRF groups: n = 3).
(I) Daily food intake (n = 4).
(J) Gene expression in liver (n = 4–5).
(K) Scheme for CPS during pregnancy and offspring mice subjected to a calorie-restricted HFD.
(L) BW of male offspring (n = 5) and a representative image.
(M) BMI and percentage of fat mass (n = 5).
(N) Representative photograph (top) and weights (n = 5, bottom) of tissues. peri, perirenal; epi, epididymal; sub, subcutaneous.
(O) Glucose (top) and insulin (bottom) tolerance tests (n = 5).
(P) AUC of glucose (top) and insulin (bottom) tolerance tests (n = 5).
(Q) Metabolic cage assessment of male offspring (n = 4).
(R) Daily food intake adjusted by BW (n = 5).
(S) Daily water intake (n = 5). L, light; D, dark.
(T) Percentage of extracellular fluid and total body water (n = 5). $^{*}p < 0.05$, $^{**}p < 0.01$, $^{***}p < 0.001$, and $^{****}p < 0.0001$ by two-way ANOVA (C and G–J). Data are presented as mean + SEM.
See also Figure S7.

STAR★METHODS

Detailed methods are provided in the online version of this paper and include the following:

- KEY RESOURCES TABLE
- EXPERIMENTAL MODEL AND STUDY PARTICIPANT DETAILS
  - Animal Experiments
- METHOD DETAILS
  - Metabolic Cage Analysis
  - Locomotor Activity Analysis
  - Body Composition Measurement
  - Serum Chemistry
  - Serum Corticosterone Quantitation
  - Serum Leptin Quantitation
  - Intraperitoneal glucose tolerance test and insulin tolerance test
  - Staining
  - Protein Extraction and Western Blot
  - Antibodies
  - RNA Extraction and Reverse Transcription
  - Quantitative real-time PCR analysis
  - RNA-sequencing
  - Metabolomics
  - Gut microbiome
  - Reduced representation bisulfite sequencing
  - Single-cell RNA-sequencing
- QUANTIFICATION AND STATISTICAL ANALYSIS
  - Metabolomics
  - Integrated metabolic pathway analysis
  - Circadian Rhythmicity Determination
  - Bioinformatic Analysis
  - Other Statistical Analyses

SUPPLEMENTAL INFORMATION

Supplemental information can be found online at https://doi.org/10.1016/j.cmet.2024.12.002.

Received: August 7, 2023
Revised: April 29, 2024
Accepted: December 4, 2024
Published: January 14, 2025

REFERENCES

1. Takahashi, J.S. (2017). Transcriptional architecture of the mammalian circadian clock. Nat. Rev. Genet. *18*, 164–179. https://doi.org/10.1038/nrg.2016.150.
2. Nagoshi, E., Saini, C., Bauer, C., Laroche, T., Naef, F., and Schibler, U. (2004). Circadian gene expression in individual fibroblasts: cell-autonomous and self-sustained oscillators pass time to daughter cells. Cell *119*, 693–705. https://doi.org/10.1016/j.cell.2004.11.015.
3. Schibler, U., and Sassone-Corsi, P. (2002). A web of circadian pacemakers. Cell *111*, 919–922.
4. Greco, C.M., Koronowski, K.B., Smith, J.G., Shi, J., Kunderfranco, P., Carriero, R., Chen, S., Samad, M., Welz, P.S., Zinna, V.M., et al. (2021). Integration of feeding behavior by the liver circadian clock reveals network dependency of metabolic rhythms. Sci. Adv. *7*, eabi7828. https://doi.org/10.1126/sciadv.abi7828.
5. Ravelli, A.C., van der Meulen, J.H., Michels, R.P., Osmond, C., Barker, D.J., Hales, C.N., and Bleker, O.P. (1998). Glucose tolerance in adults after prenatal exposure to famine. Lancet *351*, 173–177. https://doi.org/10.1016/s0140-6736(97)07244-9.
6. Yura, S., Itoh, H., Sagawa, N., Yamamoto, H., Masuzaki, H., Nakao, K., Kawamura, M., Takemura, M., Kakui, K., Ogawa, Y., and Fujii, S. (2005). Role of premature leptin surge in obesity resulting from intrauterine undernutrition. Cell Metab. *1*, 371–378. https://doi.org/10.1016/j.cmet.2005.05.005.
7. Eriksson, J.G., Sandboge, S., Salonen, M., Kajantie, E., and Osmond, C. (2015). Maternal weight in pregnancy and offspring body composition in late adulthood: findings from the Helsinki Birth Cohort Study (HBCS). Ann. Med. *47*, 94–99. https://doi.org/10.3109/07853890.2015.1004360.
8. Hales, C.N., and Barker, D.J. (1992). Type 2 (non-insulin-dependent) diabetes mellitus: the thrifty phenotype hypothesis. Diabetologia *35*, 595–601. https://doi.org/10.1007/BF00400248.
9. Bates, K., and Herzog, E.D. (2020). Maternal-Fetal Circadian Communication During Pregnancy. Front. Endocrinol. *11*, 198. https://doi.org/10.3389/fendo.2020.00198.
10. Lassi, M., Tomar, A., Comas-Armangué, G., Vogtmann, R., Dijkstra, D.J., Corujo, D., Gerlini, R., Darr, J., Scheid, F., Rozman, J., et al. (2021). Disruption of paternal circadian rhythm affects metabolic health in male offspring via nongerm cell factors. Sci. Adv. *7*, eabg6424. https://doi.org/10.1126/sciadv.abg6424.
11. Astiz, M., Heyde, I., Fortmann, M.I., Bossung, V., Roll, C., Stein, A., Grüttner, B., Göpel, W., Härtel, C., Obleser, J., et al. (2020). The circadian phase of antenatal glucocorticoid treatment affects the risk of behavioral disorders. Nat. Commun. *11*, 3593. https://doi.org/10.1038/s41467-020-17429-5.
12. Kimura, I., Miyamoto, J., Ohue-Kitano, R., Watanabe, K., Yamada, T., Onuki, M., Aoki, R., Isobe, Y., Kashihara, D., Inoue, D., et al. (2020). Maternal gut microbiota in pregnancy influences offspring metabolic phenotype in mice. Science *367*, eaaw8429. https://doi.org/10.1126/science.aaw8429.
13. Hsu, C.N., and Tain, Y.L. (2020). Light and Circadian Signaling Pathway in Pregnancy: Programming of Adult Health and Disease. Int. J. Mol. Sci. *21*, 2232. https://doi.org/10.3390/ijms21062232.
14. Yamaguchi, Y., and Okamura, H. (2018). Vasopressin Signal Inhibition in Aged Mice Decreases Mortality under Chronic Jet Lag. iScience *5*, 118–122. https://doi.org/10.1016/j.isci.2018.06.008.
15. Arble, D.M., Bass, J., Laposky, A.D., Vitaterna, M.H., and Turek, F.W. (2009). Circadian timing of food intake contributes to weight gain. Obesity *17*, 2100–2102. https://doi.org/10.1038/oby.2009.264.
16. Hepler, C., Weidemann, B.J., Waldeck, N.J., Marcheva, B., Cedernaes, J., Thorne, A.K., Kobayashi, Y., Nozawa, R., Newman, M.V., Gao, P., et al. (2022). Time-restricted feeding mitigates obesity through adipocyte thermogenesis. Science *378*, 276–284. https://doi.org/10.1126/science.abl8007.
17. Kohsaka, A., Laposky, A.D., Ramsey, K.M., Estrada, C., Joshu, C., Kobayashi, Y., Turek, F.W., and Bass, J. (2007). High-fat diet disrupts behavioral and molecular circadian rhythms in mice. Cell Metab. *6*, 414–421. https://doi.org/10.1016/j.cmet.2007.09.006.
18. Turek, F.W., Joshu, C., Kohsaka, A., Lin, E., Ivanova, G., McDearmon, E., Laposky, A., Losee-Olson, S., Easton, A., Jensen, D.R., et al. (2005). Obesity and metabolic syndrome in circadian Clock mutant mice. Science *308*, 1043–1045. https://doi.org/10.1126/science.1108750.
19. Eckel-Mahan, K.L., Patel, V.R., de Mateo, S., Orozco-Solis, R., Ceglia, N.J., Sahar, S., Dilag-Penilla, S.A., Dyar, K.A., Baldi, P., and Sassone-Corsi, P. (2013). Reprogramming of the circadian clock by nutritional challenge. Cell *155*, 1464–1478. https://doi.org/10.1016/j.cell.2013.11.034.
20. Guan, D., Xiong, Y., Borck, P.C., Jang, C., Doulias, P.T., Papazyan, R., Fang, B., Jiang, C., Zhang, Y., Briggs, E.R., et al. (2018). Diet-Induced Circadian Enhancer Remodeling Synchronizes Opposing Hepatic Lipid Metabolic Processes. Cell *174*, 831–842.e12. https://doi.org/10.1016/j.cell.2018.06.031.
21. Kettner, N.M., Mayo, S.A., Hua, J., Lee, C., Moore, D.D., and Fu, L. (2015). Circadian Dysfunction Induces Leptin Resistance in Mice. Cell Metab. *22*, 448–459. https://doi.org/10.1016/j.cmet.2015.06.005.
22. Paschos, G.K., Ibrahim, S., Song, W.L., Kunieda, T., Grant, G., Reyes, T.M., Bradfield, C.A., Vaughan, C.H., Eiden, M., Masoodi, M., et al.

(2012). Obesity in mice with adipocyte-specific deletion of clock component Arntl. Nat. Med. *18*, 1768–1777. https://doi.org/10.1038/nm.2979.

23. Dyar, K.A., Lutter, D., Artati, A., Ceglia, N.J., Liu, Y., Armenta, D., Jastroch, M., Schneider, S., de Mateo, S., Cervantes, M., et al. (2018). Atlas of Circadian Metabolism Reveals System-wide Coordination and Communication between Clocks. Cell *174*, 1571–1585.e11. https://doi.org/10.1016/j.cell.2018.08.042.
24. Kinouchi, K., Magnan, C., Ceglia, N., Liu, Y., Cervantes, M., Pastore, N., Huynh, T., Ballabio, A., Baldi, P., Masri, S., and Sassone-Corsi, P. (2018). Fasting Imparts a Switch to Alternative Daily Pathways in Liver and Muscle. Cell Rep. *25*, 3299–3314.e6. https://doi.org/10.1016/j.celrep.2018.11.077.
25. Tognini, P., Murakami, M., Liu, Y., Eckel-Mahan, K.L., Newman, J.C., Verdin, E., Baldi, P., and Sassone-Corsi, P. (2017). Distinct Circadian Signatures in Liver and Gut Clocks Revealed by Ketogenic Diet. Cell Metab. *26*, 523–538.e5. https://doi.org/10.1016/j.cmet.2017.08.015.
26. Jeyaraj, D., Scheer, F.A.J.L., Ripperger, J.A., Haldar, S.M., Lu, Y., Prosdocimo, D.A., Eapen, S.J., Eapen, B.L., Cui, Y., Mahabeleshwar, G.H., et al. (2012). Klf15 orchestrates circadian nitrogen homeostasis. Cell Metab. *15*, 311–323. https://doi.org/10.1016/j.cmet.2012.01.020.
27. Koronowski, K.B., Kinouchi, K., Welz, P.S., Smith, J.G., Zinna, V.M., Shi, J., Samad, M., Chen, S., Magnan, C.N., Kinchen, J.M., et al. (2019). Defining the Independence of the Liver Circadian Clock. Cell *177*, 1448–1462.e14. https://doi.org/10.1016/j.cell.2019.04.025.
28. Pang, Z., Chong, J., Zhou, G., de Lima Morais, D.A., Chang, L., Barrette, M., Gauthier, C., Jacques, P.É., Li, S., and Xia, J. (2021). MetaboAnalyst 5.0: narrowing the gap between raw spectra and functional insights. Nucleic Acids Res. *49*, W388–W396. https://doi.org/10.1093/nar/gkab382.
29. Tuganbaev, T., Mor, U., Bashiardes, S., Liwinski, T., Nobs, S.P., Leshem, A., Dori-Bachash, M., Thaiss, C.A., Pinker, E.Y., Ratiner, K., et al. (2020). Diet Diurnally Regulates Small Intestinal Microbiome-Epithelial-Immune Homeostasis and Enteritis. Cell *182*, 1441–1459.e21. https://doi.org/10.1016/j.cell.2020.08.027.
30. Zarrinpar, A., Chaix, A., Yooseph, S., and Panda, S. (2014). Diet and feeding pattern affect the diurnal dynamics of the gut microbiome. Cell Metab. *20*, 1006–1017. https://doi.org/10.1016/j.cmet.2014.11.008.
31. Astiz, M., and Oster, H. (2020). Feto-Maternal Crosstalk in the Development of the Circadian Clock System. Front. Neurosci. *14*, 631687. https://doi.org/10.3389/fnins.2020.631687.
32. Okabayashi, N., Yasuo, S., Watanabe, M., Namikawa, T., Ebihara, S., and Yoshimura, T. (2003). Ontogeny of circadian clock gene expression in the pineal and the suprachiasmatic nucleus of chick embryo. Brain Res. *990*, 231–234. https://doi.org/10.1016/s0006-8993(03)03531-5.
33. Yagita, K., Horie, K., Koinuma, S., Nakamura, W., Yamanaka, I., Urasaki, A., Shigeyoshi, Y., Kawakami, K., Shimada, S., Takeda, J., and Uchiyama, Y. (2010). Development of the circadian oscillator during differentiation of mouse embryonic stem cells *in vitro*. Proc. Natl. Acad. Sci. USA *107*, 3846–3851. https://doi.org/10.1073/pnas.0913256107.
34. Yuan, X., Tsujimoto, K., Hashimoto, K., Kawahori, K., Hanzawa, N., Hamaguchi, M., Seki, T., Nawa, M., Ehara, T., Kitamura, Y., et al. (2018). Epigenetic modulation of Fgf21 in the perinatal mouse liver ameliorates diet-induced obesity in adulthood. Nat. Commun. *9*, 636. https://doi.org/10.1038/s41467-018-03038-w.
35. Yamaguchi, Y., Suzuki, T., Mizoro, Y., Kori, H., Okada, K., Chen, Y., Fustin, J.M., Yamazaki, F., Mizuguchi, N., Zhang, J., et al. (2013). Mice genetically deficient in vasopressin V1a and V1b receptors are resistant to jet lag. Science *342*, 85–90. https://doi.org/10.1126/science.1238599.
36. Hemberger, M., Hanna, C.W., and Dean, W. (2020). Mechanisms of early placental development in mouse and humans. Nat. Rev. Genet. *21*, 27–43. https://doi.org/10.1038/s41576-019-0169-4.
37. Rossant, J., and Cross, J.C. (2001). Placental development: lessons from mouse mutants. Nat. Rev. Genet. *2*, 538–548. https://doi.org/10.1038/35080570.
38. Fowden, A.L., Sferruzzi-Perri, A.N., Coan, P.M., Constancia, M., and Burton, G.J. (2009). Placental efficiency and adaptation: endocrine regulation. J. Physiol. *587*, 3459–3472. https://doi.org/10.1113/jphysiol.2009.173013.
39. Marsh, B., and Blelloch, R. (2020). Single nuclei RNA-seq of mouse placental labyrinth development. eLife *9*, e60266. https://doi.org/10.7554/eLife.60266.
40. Hatori, M., Vollmers, C., Zarrinpar, A., DiTacchio, L., Bushong, E.A., Gill, S., Leblanc, M., Chaix, A., Joens, M., Fitzpatrick, J.A.J., et al. (2012). Time-restricted feeding without reducing caloric intake prevents metabolic diseases in mice fed a high-fat diet. Cell Metab. *15*, 848–860. https://doi.org/10.1016/j.cmet.2012.04.019.
41. Acosta-Rodríguez, V.A., de Groot, M.H.M., Rijo-Ferreira, F., Green, C.B., and Takahashi, J.S. (2017). Mice under Caloric Restriction Self-Impose a Temporal Restriction of Food Intake as Revealed by an Automated Feeder System. Cell Metab. *26*, 267–277.e2. https://doi.org/10.1016/j.cmet.2017.06.007.
42. Kinouchi, K., and Sassone-Corsi, P. (2020). Metabolic rivalry: circadian homeostasis and tumorigenesis. Nat. Rev. Cancer *20*, 645–661. https://doi.org/10.1038/s41568-020-0291-9.
43. Welz, P.S., Zinna, V.M., Symeonidi, A., Koronowski, K.B., Kinouchi, K., Smith, J.G., Guillén, I.M., Castellanos, A., Furrow, S., Aragón, F., et al. (2019). BMAL1-Driven Tissue Clocks Respond Independently to Light to Maintain Homeostasis. Cell *177*, 1436–1447.e12. https://doi.org/10.1016/j.cell.2019.05.009.
44. Umemura, Y., Koike, N., Ohashi, M., Tsuchiya, Y., Meng, Q.J., Minami, Y., Hara, M., Hisatomi, M., and Yagita, K. (2017). Involvement of posttranscriptional regulation of Clock in the emergence of circadian clock oscillation during mouse development. Proc. Natl. Acad. Sci. USA *114*, E7479–E7488. https://doi.org/10.1073/pnas.1703170114.
45. Sato, S., Hishida, T., Kinouchi, K., Hatanaka, F., Li, Y., Nguyen, Q., Chen, Y., Wang, P.H., Kessenbrock, K., Li, W., et al. (2023). The circadian clock CRY1 regulates pluripotent stem cell identity and somatic cell reprogramming. Cell Rep. *42*, 112590. https://doi.org/10.1016/j.celrep.2023.112590.
46. Alvarez-Dominguez, J.R., Donaghey, J., Rasouli, N., Kenty, J.H.R., Helman, A., Charlton, J., Straubhaar, J.R., Meissner, A., and Melton, D.A. (2020). Circadian Entrainment Triggers Maturation of Human In Vitro Islets. Cell Stem Cell *26*, 108–122.e10. https://doi.org/10.1016/j.stem.2019.11.011.
47. Kondratov, R.V., Kondratova, A.A., Gorbacheva, V.Y., Vykhovanets, O.V., and Antoch, M.P. (2006). Early aging and age-related pathologies in mice deficient in BMAL1, the core componentof the circadian clock. Genes Dev. *20*, 1868–1873. https://doi.org/10.1101/gad.1432206.
48. Yang, G., Chen, L., Grant, G.R., Paschos, G., Song, W.L., Musiek, E.S., Lee, V., McLoughlin, S.C., Grosser, T., Cotsarelis, G., and FitzGerald, G.A. (2016). Timing of expression of the core clock gene Bmal1 influences its effects on aging and survival. Sci. Transl. Med. *8*, 324ra16. https://doi.org/10.1126/scitranslmed.aad3305.
49. Canaple, L., Gréchez-Cassiau, A., Delaunay, F., Dkhissi-Benyahya, O., and Samarut, J. (2018). Maternal eating behavior is a major synchronizer of fetal and postnatal peripheral clocks in mice. Cell. Mol. Life Sci. *75*, 3991–4005. https://doi.org/10.1007/s00018-018-2845-5.
50. Carmona-Alcocer, V., Abel, J.H., Sun, T.C., Petzold, L.R., Doyle, F.J., 3rd, Simms, C.L., and Herzog, E.D. (2018). Ontogeny of Circadian Rhythms and Synchrony in the Suprachiasmatic Nucleus. J. Neurosci. *38*, 1326–1334. https://doi.org/10.1523/JNEUROSCI.2006-17.2017.
51. Reppert, S.M., and Schwartz, W.J. (1986). Maternal suprachiasmatic nuclei are necessary for maternal coordination of the developing circadian system. J. Neurosci. *6*, 2724–2729. https://doi.org/10.1523/JNEUROSCI.06-09-02724.1986.
52. Pena-Leon, V., Folgueira, C., Barja-Fernández, S., Pérez-Lois, R., Da Silva Lima, N., Martin, M., Heras, V., Martinez-Martinez, S., Valero, P., Iglesias, C., et al. (2022). Prolonged breastfeeding protects from obesity by hypothalamic action of hepatic FGF21. Nat. Metab. *4*, 901–917. https://doi.org/10.1038/s42255-022-00602-z.

53. Schneider, C.A., Rasband, W.S., and Eliceiri, K.W. (2012). NIH Image to ImageJ: 25 years of image analysis. Nat. Methods *9*, 671–675. https://doi.org/10.1038/nmeth.2089.

54. Pang, Z., Lu, Y., Zhou, G., Hui, F., Xu, L., Viau, C., Spigelman, A.F., MacDonald, P.E., Wishart, D.S., Li, S., and Xia, J. (2024). MetaboAnalyst 6.0: towards a unified platform for metabolomics data processing, analysis and interpretation. Nucleic Acids Res. *52*, W398–W406. https://doi.org/10.1093/nar/gkae253.

55. Hughes, M.E., Hogenesch, J.B., and Kornacker, K. (2010). JTK_CYCLE: An Efficient Nonparametric Algorithm for Detecting Rhythmic Components in Genome-Scale Data Sets. J. Biol. Rhythms *25*, 372–380. https://doi.org/10.1177/0748730410379711.

56. Huang da, W., Sherman, B.T., and Lempicki, R.A. (2009). Systematic and integrative analysis of large gene lists using DAVID bioinformatics resources. Nat. Protoc. *4*, 44–57. https://doi.org/10.1038/nprot.2008.211.

57. Baldi, P., and Long, A.D. (2001). A Bayesian framework for the analysis of microarray expression data: regularized t -test and statistical inferences of gene changes. Bioinformatics *17*, 509–519.

58. Kayala, M.A., and Baldi, P. (2012). Cyber-T web server: differential analysis of high-throughput data. Nucleic Acids Res. *40*, W553–W559. https://doi.org/10.1093/nar/gks420.

59. Patel, V.R., Eckel-Mahan, K., Sassone-Corsi, P., and Baldi, P. (2012). CircadiOmics: integrating circadian genomics, transcriptomics, proteomics and metabolomics. Nat. Methods *9*, 772–773. https://doi.org/10.1038/nmeth.2111.

60. Smith, D., Jr., Johnson, M., and Nagy, T. (2009). Precision and accuracy of bioimpedance spectroscopy for determination of in vivo body composition in rats. Int. J. Body Compos. Res. *7*, 21–26.

61. Nishad, A., Naseem, A., Rani, S., and Malik, S. (2023). Automated qualitative batch measurement of lipid droplets in the liver of bird using ImageJ. Star Protoc. *4*, 102466. https://doi.org/10.1016/j.xpro.2023.102466.

62. Hosomi, K., Saito, M., Park, J., Murakami, H., Shibata, N., Ando, M., Nagatake, T., Konishi, K., Ohno, H., Tanisawa, K., et al. (2022). Oral administration of Blautia wexlerae ameliorates obesity and type 2 diabetes via metabolic remodeling of the gut microbiota. Nat. Commun. *13*, 4477. https://doi.org/10.1038/s41467-022-32015-7.

63. Sánchez-Pérez, S., Comas-Basté, O., Duelo, A., Veciana-Nogués, M.T., Berlanga, M., Latorre-Moratalla, M.L., and Vidal-Carou, M.C. (2022). Intestinal dysbiosis in patients with histamine intolerance. Nutrients *14*, 1774. https://doi.org/10.3390/nu14091774.

64. Hao, Y., Hao, S., Andersen-Nissen, E., Mauck, W.M., 3rd, Zheng, S., Butler, A., Lee, M.J., Wilk, A.J., Darby, C., Zager, M., et al. (2021). Integrated analysis of multimodal single-cell data. Cell *184*, 3573–3587.e29. https://doi.org/10.1016/j.cell.2021.04.048.

65. Young, M.D., and Behjati, S. (2020). SoupX removes ambient RNA contamination from droplet-based single-cell RNA sequencing data. GigaScience *9*, giaa151. https://doi.org/10.1093/gigascience/giaa151.

66. McGinnis, C.S., Murrow, L.M., and Gartner, Z.J. (2019). DoubletFinder: Doublet Detection in Single-Cell RNA Sequencing Data Using Artificial Nearest Neighbors. Cell Syst. *8*, 329–337.e4. https://doi.org/10.1016/j.cels.2019.03.003.

67. Agostinelli, F., Ceglia, N., Shahbaba, B., Sassone-Corsi, P., and Baldi, P. (2016). What time is it? Deep learning approaches for circadian rhythms. Bioinformatics *32*, i8–i17. https://doi.org/10.1093/bioinformatics/btw243.

68. Samad, M., Agostinelli, F., Sato, T., Shimaji, K., and Baldi, P. (2022). CircadiOmics: circadian omic web portal. Nucleic Acids Res. *50*, W183–W190. https://doi.org/10.1093/nar/gkac419.

STAR★METHODS

KEY RESOURCES TABLE

REAGENT or RESOURCE	SOURCE	IDENTIFIER
Antibodies		
Rabbit polyclonal anti-BMAL1	Abcam	Cat# ab93806; RRID:AB_10675117
Rabbit monoclonal anti-REV-ERBα	Cell Signaling Technology	Cat#13418; RRID:AB_2630359
Rabbit polyclonal anti-PER2	Alpha Diagnostic International	Cat# PER21-A; RRID:AB_1620951
Rabbit polyclonal anti-CRY1	Bethyl Laboratories	Cat# A302-614A; RRID:AB_10555376
Rabbit polyclonal anti-β-ACTIN	Cell Signaling Technology	Cat# 4967; RRID:AB_330288
Rabbit polyclonal anti-AKT	Cell Signaling Technology	Cat# 9272; RRID:AB_329827
Rabbit monoclonal anti-P-AKT	Cell Signaling Technology	Cat# 4060; RRID:AB_2315049
Rabbit polyclonal anti-MAPK	Cell Signaling Technology	Cat# 9102; RRID:AB_330744
Rabbit polyclonal anti-P-MAPK	Cell Signaling Technology	Cat# 9101; RRID:AB_331646
Rabbit monoclonal anti-AMPK	Cell Signaling Technology	Cat# 2603; RRID:AB_490795
Rabbit monoclonal anti-P-AMPK	Cell Signaling Technology	Cat# 2535; RRID:AB_331250
Rabbit monoclonal anti-STAT3	Cell Signaling Technology	Cat# 4904; RRID:AB_331269
Rabbit polyclonal anti-P-STAT3	Cell Signaling Technology	Cat# 9131; RRID:AB_331586
Polyclonal Goat anti-Rabbit-IgG	Sigma-Aldrich	Cat# 12-348; RRID:AB_390191
Rabbit monoclonal anti-F4/80	Cell Signaling Technology	Cat# 70076; RRID:AB_2799771
Chemicals, peptides, and recombinant proteins		
Tamoxifen	Sigma	T5648
Insulin (Humulin R 100U/mL)	Eli Lilly	N/A
0.9% NaCl	Otsuka	CA-7647-14-5
20% Glucose injection	Otsuka	CAS-50-99-7
4% Paraformaldehyde Phosphate Buffer Solution	Fujifilm	163-20145
Chemiluminescent HRP substrate	EMD Millipore	WBKLS0500
TRIzol reagent	Invitrogen	15596018
QIAzol lysis reagent	Qiagen	79306
iScript cDNA synthesis kit	Bio-Rad Laboratories	1708891
SsoAdvanced Universal SYBR Green Supermix	Bio-Rad Laboratories	1725271
RNeasy plus mini kit	Qiagen	74134
Protease inhibitor cocktail	Roche	11697498001
Critical commercial assays		
Leptin ELISA kit	Morinaga Institute of Biological Science, Inc	M1305
StatStrip Xpress glucometer	Nova Biomedical	N/A
Corticosterone ELISA kit	Enzo Life Sciences Inc	ADI-900-097
Deposited data		
RNA-sequencing	GEO	GEO: GSE236201
Single-cell RNA-sequencing	GEO	GEO: GSE235916
Metabolomics	This paper	Table S1
16S rRNA gene amplicon sequencing analysis	SRA	PRJNA1096943
DNA methylation analysis	GEO	GEO: GSE263993
Source Data	This paper	Data S1
Experimental models: Organisms/strains		
Mouse: C57BL/6J	CLEA Japan Inc.	C57BL/6JJcl
Mouse: Bmal1$^{flox/flox}$	The Jackson Laboratory	B6.129S4(Cg)-Bmal1^{tm1Weit}/J; RRID:IMSR_JAX:007668

(*Continued on next page*)

Continued

REAGENT or RESOURCE	SOURCE	IDENTIFIER
Mouse: CAG-CreER$^{+/-}$	The Jackson Laboratory	B6.Cg-Tg(CAG-cre/Esr1*)5Amc/J; RRID:IMSR_JAX:004682
Oligonucleotides		
qPCR primers	This paper	Table S5
Software and algorithms		
Actmaster software	Melquest	https://www.melquest.jp/products/products-1299/
ImageJ software	Schneider et al.[53]	https://imagej.net/ij/index.html
MetaboAnalyst 6.0	Pang et al.[54]	https://www.metaboanalyst.ca/
JTK_CYCLE	Hughes et al.[55]	N/A
DAVID	Huang et al.[56]	https://david-d.ncifcrf.gov/
Cyber-T	Baldi and Long[57]; Kayala and Baldi[58]	https://cybert.ics.uci.edu/
Circadiomics	Patel et al.[59]	http://circadiomics.igb.uci.edu/
GraphPad Prism 10	GraphPad	https://www.graphpad.com/scientific-software/prism/
Metabolon's Integrated Bioinformatics Platform	Metabolon.com	https://www.metabolon.com/bioinformatics/
BioRender	BioRender.com (2023)	https://app.biorender.com/biorender-templates
Other		
Standard chow	CLEA Japan	CE-2
High fat diet	Research Diets	D12492
Low fat diet	Research Diets	D12450J
Automated feeder system	Melquest	FDBR-300
Metabolic cages	ARCO SYSTEM Inc.	ARCO-2000
Optical beam motion detector	Melquest	LS-5
Data acquisition and recording system	Melquest	CIF-4A
Bioimpedance spectroscopy device	ImpediMed Inc.	VET BIS1
Dry-chemistry analyzer	Fujifilm	DRI-CHEM NX500V
3CCD camera	Keyence	BZ-X800
Imaging system	Fujifilm	LAS-4000 Mini
QuantStudio™ 5 Real-Time PCR System	Thermo Fisher Scientific	A34322

EXPERIMENTAL MODEL AND STUDY PARTICIPANT DETAILS

Animal Experiments

Six- to eight-week-old C57BL/6J male and female mice (CLEA Japan, Inc., Tokyo, Japan) were fed with a standard chow (CE-2; CLEA Japan, Inc., Tokyo, Japan) and bred under a temperature-controlled (temperatures of 66-75°F), 12 h LD schedule. Following confirmation of the plugs, putatively pregnant mice were randomly divided and housed under either the control LD condition (CON) or the CPS condition, where the phase was advanced by 8 h every 5 days exclusively during pregnancy. Four-week-old male and female offspring mice were fed *ad libitum* with either an HFD (with 60 kcal% fat, D12492, Research Diets, New Brunswick, USA) or an LFD (D12450J, Research Diets, New Brunswick, USA) for 12 weeks and housed individually. Tissues were collected over a circadian cycle at ZT0, ZT6, ZT12, and ZT18 (n = 5-7 per time point in each group). For the TRF experiment, 4-week-old male offspring mice were subjected to temporal feeding restriction of HFD exclusively during the 12 h dark phase using the automated feeder system (Melquest, Toyama, Japan) for 12 weeks. Samples were collected at ZT0 and ZT12 (n=4-7 per time point in each group). With regard to the caloric restriction (CR) experiment, the food consumption of *ad libitum* HFD feeding in the offspring born to the CON mothers were measured twice a week from the age of four to sixteen weeks. The HFD equivalent to 60% of the calorie taken on the *ad libitum* feeding condition were given at ZT12 daily to the CON and CPS offspring at their corresponding ages. Samples were collected at ZT12 (n=5 per time point in each group).

Six- to eight-week-old of *Bmal1*$^{flox/flox}$ mice (007668, the Jackson Laboratory, United States) and CAG-CreER$^{+/-}$ mice (004682, the Jackson Laboratory, United States) were bred over three generations to obtain *Bmal1*$^{flox/flox}$; CAG-CreER$^{+/-}$ (BKO) mice under the LD

condition. Female BKO mice were bred with male *Bmal1*$^{flox/flox}$; CAG-CreER$^{-/-}$ (WT) mice in the experimental group, and male BKO mice were bred with female WT mice in the control group. Immediately after the plug was confirmed in a female mouse, the pregnant mouse was moved to an isolator with LD cycles and administered an oral gavage of tamoxifen (T5648, Sigma, St. Louis, USA) from E7.5 to E11.5 with a dosage of 50 mg/kg/day. After E11.5, pregnant female mice were housed in constant darkness. The offspring mice with the *Bmal1*$^{flox/flox}$; CAG-CreER$^{-/-}$ genotype were challenged with LFD and HFD as described in CON and CPS offspring.

Following confirmation of the plugs (E0.5), the tissues of pregnant maternal mice of the CON, CPS, WT and BKO groups were harvested on the embryonic day 18.5 (E18.5). To investigate the effect of circadian disruption prior to pregnancy, four-week-old female mice were subjected to the CPS condition for three weeks (CPS-BP). The CPS-BP mice were bred with male mice under a temperature-controlled, 12 h LD schedule and the tissues were collected at ZT12 on E18.5. To explore whether the circadian disruption from mid-way to the end of pregnancy is sufficient to cause the phenotype of the offspring, CPS was implemented exclusively for the latter two-thirds of pregnancy (2/3CPS) and the tissues were harvested at ZT12 on E18.5.

The mouse samples were randomly selected from each group for the subsequent analyses. The body weight of offspring mice was measured every week unless the animals were subjected to experiments such as the body composition analysis, metabolic cage analysis, as well as glucose and insulin tolerance tests. All animal experiments were designed and performed in accordance with the guidelines for animal experimentation of the Keio University School of Medicine.

METHOD DETAILS

Metabolic Cage Analysis

The offspring mice aged from 14 to 16 weeks were monitored individually in metabolic cages (ARCO-2000; ARCO SYSTEM Inc., Kashiwa, Japan.) with *ad libitum*, nighttime-restricted, or calorie-restricted access to food and *ad libitum* access to drinking water for 72 h. Each cage was monitored for respiratory quotient (RQ), energy expenditure, oxygen consumption (VO2), and carbon dioxide production (VCO2) at 5-min intervals for 72 h, with the first day reserved to acclimatize the mice to the cage environment.

Locomotor Activity Analysis

Locomotor activity was measured in pregnant maternal mice or offspring mice using an optical beam motion detector LS-5 (Melquest, Toyama, Japan). Data were collected using a CIF-4A data acquisition and recording system (Melquest, Toyama, Japan). Actograms and activity profiles were computed using the Actmaster software (Melquest, Toyama, Japan).

Body Composition Measurement

Body mass index, fat mass, total body water amount, and extracellular fluid of 14- to 16-week-old offspring were measured using a bioimpedance technology with ImpediVET (ImpediMed Inc., Carlsbad, CA, USA). The *in vivo* body composition of animals determined using ImpediVET correlated well with the chemical carcass analysis of the total body water amount.[60] All the measurements were performed during a constant 2-h period (from 7 to 9 pm).

Serum Chemistry

Serum TC and TG levels were determined using a DRI-CHEM NX500V analyzer (FujiFilm, Tokyo, Japan).

Serum Corticosterone Quantitation

The serum samples were collected over a circadian cycle at ZT0, ZT6, ZT12, and ZT18 from the pregnant maternal mice on E18.5. Serum corticosterone levels were quantified using a Corticosterone ELISA Kit (ADI-900-097, Enzo Life Sciences Inc, NY, USA) according to the manufacturer's instructions (n=4 samples per time point per group).

Serum Leptin Quantitation

The serum samples were collected over a circadian cycle at ZT0, ZT6, ZT12, and ZT18 from the offspring mice aged from 15 to 16 weeks, and at ZT0 and ZT12 from the four-week-old offspring mice. Serum leptin levels were quantified using a Leptin ELISA Kit (M1305, Morinaga Institute of Biological Science, Inc, Yokohama, Japan) according to the manufacturer's instructions (n=4–5 samples per time point per group).

Intraperitoneal glucose tolerance test and insulin tolerance test

Intraperitoneal glucose tolerance test was performed following 12 h of fasting with *ad libitum* access to water in the offspring mice aged from 15 to 16 weeks. 2 g of glucose/kg body weight was intraperitoneally administered at an injection volume of 0.1 mL/10 g body weight (27 G needle and 1 cc syringe). The insulin tolerance test was performed following 2 h of fasting with *ad libitum* access to water in the offspring mice aged from 15 to 16 weeks. Insulin was diluted to 1 U/kg in sterile saline buffer (0.9% NaCl). Blood glucose levels were measured at 0, 30, 60, 90, 120 min following the glucose or insulin administration, using a glucometer (Nova Biomedical, Waltham, USA) by applying a drop of free-flowing blood onto a new test strip.

Staining

Formalin-fixed paraffin-embedded tissues were sectioned at 4-μm thickness and used for hematoxylin and eosin (H&E) staining (liver, WAT, and placenta), oil red O staining (liver), and immunohistochemical analysis of F4/80 (WAT). Photographs of the stained sections were obtained, and adipocyte size was quantified using a 3CCD camera (BZ-X800, Keyence, Osaka, Japan). F4/80 positive cells were counted using the ImageJ software.[53] Percentage of positive oil red O staining in the liver were measured using the ImageJ software as previously described.[61]

Protein Extraction and Western Blot

Frozen tissues were homogenized in modified radioimmunoprecipitation assay buffer (50 mM Tris-HCl [pH 8.0], 150 mM NaCl, 5 mM EDTA, 1% NP-40, and 15 mM $MgCl_2$) supplemented with Protease Inhibitor Cocktail (Roche, Mannheim, Germany), NaF and PMSF, sonicated briefly and rocked to lyse cells at 4°C. Samples were centrifuged at 15000 rpm for 15 min at 4°C. Supernatants were stored as whole-cell protein lysates. Protein lysates (5-60 μg) were separated on 6%–10% gels using SDS-PAGE and transferred to nitrocellulose membranes. The membranes were incubated with primary antibodies and peroxidase-conjugated secondary antibodies at 4°C and visualized by chemiluminescent HRP substrate (WBKLS0500, EMD Millipore, Massachusetts, USA). The blots were detected by chemiluminescence and scanned using an imaging system (LAS-4000 Mini, Fujifilm, Tokyo, Japan).

Antibodies

The antibodies used for western blotting were as follows: BMAL1 (ab93806, Abcam, 1:10000), REV-ERBα (#13418, Cell Signaling Technology, 1:1000), PER2 (PER21-A, Alpha Diagnostic International, 1:1000), CRY1 (A302-614A, Bethyl Laboratories, 1:2000), P-AKT (#4060, Cell Signaling Technology, 1:2000), AKT (#9272, Cell Signaling Technology, 1:1000), P-MAPK (#9101, Cell Signaling Technology, 1:1000), MAPK (#9102, Cell Signaling Technology, 1:1000), P-AMPK (#2535, Cell Signaling Technology, 1:1000), AMPK (#2603, Cell Signaling Technology, 1:1000), P-STAT3 (#9131, Cell Signaling Technology, 1:1000), STAT3 (#4904, Cell Signaling Technology, 1:2000), β-ACTIN (#4967, Cell Signaling Technology, 1:5000), and secondary antibodies (12-348, Sigma-Aldrich, 1:10000) were used. Anti-F4/80 antibody (#70076, Cell Signaling Technology, 1:125) was used for immunohistochemistry.

RNA Extraction and Reverse Transcription

Total RNA was extracted from the tissues using the TRIzol reagent (Invitrogen, Carlsbad, CA, USA), followed by precipitation with isopropanol and ethanol. Total RNA was extracted from the adipose tissue using QIAzol (Qiagen, Hilden, Germany) followed by purification using the RNeasy Plus Mini Kit (Qiagen, Hilden, Germany). Complimentary DNA (cDNA) was obtained by reverse transcription of 1 μg RNA using iScript cDNA Synthesis Kit (Bio-Rad Laboratories, California, USA).

Quantitative real-time PCR analysis

cDNA was used for quantitative real-time PCR (RT-qPCR) using fluorescent dye reagent (SsoAdvanced Universal SYBR Green Supermix, Bio-Rad Laboratories, California, USA) and QuantStudio™ 5 Real-Time PCR System (A34322, Thermo Fisher Scientific, MA, USA). The mRNA levels were measured and normalized to 18S ribosomal RNA levels. All gene expression levels are presented as relative expression levels. The primer sequences are listed in Table S5.

RNA-sequencing

Total RNA was monitored for quality control using the Agilent Bioanalyzer Nano RNA chip and Nanodrop absorbance ratios for 260/280 nm and 260/230 nm. Library construction was performed according to the Illumina TruSeq mRNA stranded protocol. The input quantity for total RNA was ~1 μg and mRNA was enriched using oligo dT magnetic beads. The enriched mRNA was chemically fragmented for three minutes. First strand synthesis used random primers and reverse transcriptase to make cDNA. After second strand synthesis the ds cDNA was cleaned using AMPure XP beads and the cDNA end repaired followed by adenylation of the 3' ends. Illumina unique dual indexed adapters were ligated on the ends and the adapter ligated fragments were enriched by nine cycles of PCR. The resulting libraries were validated by qPCR and sized by Agilent Bioanalyzer DNA high sensitivity chip. The concentrations for the libraries were normalized and multiplexed together. The multiplexed libraries were sequenced using paired end 100 cycles chemistry on the NovaSeq 6000 with a target 40M reads per library. The FastQ files went through the Tuxedo protocol using Tophat and Cufflinks. Tophat was aligned to the mouse genome assembly mm10 with Bowtie2, and Cufflinks, set with a max-bundle-frags of 15000000, calculated the gene expression levels. The protocol gave us FPKM values for each gene in every replicate.

Metabolomics

Non-targeted metabolite profiling, peak identification, and curation was performed by Metabolon (Durham, NC, USA). Samples were prepared using the automated MicroLab STAR® system from Hamilton Company (Reno, NV). Several recovery standards were added prior to the first step in the extraction process for QC purposes. To remove protein, dissociate small molecules bound to protein or trapped in the precipitated protein matrix, and to recover chemically diverse metabolites, proteins were precipitated with methanol under vigorous shaking for 2 min (Glen Mills GenoGrinder 2000, New Jersey, USA) followed by centrifugation. The resulting extract was divided into five fractions: two for analysis by two separate reverse phases (RP)/UPLC-MS/MS methods with positive ion mode electrospray ionization (ESI), one for analysis by RP/UPLC-MS/MS with negative ion mode ESI, one for analysis by

HILIC/UPLC-MS/MS with negative ion mode ESI, and one sample was reserved for backup. Samples were placed briefly on a TurboVap® (Zymark, MA, USA) to remove the organic solvent. The sample extracts were stored overnight under nitrogen before preparation for analysis. Raw data was extracted, peak-identified and QC processed using Metabolon's hardware and software. Compounds were identified by comparison to a library based on authenticated standards that contains the retention time/index (RI), mass to charge ratio (*m/z*), and chromatographic data (including MS/MS spectral data). Peaks were quantified using area-under-the-curve. Batch-normalized-Imputed Data and Log-Transformed Data were used for statistical analyses.

Gut microbiome

Genomic DNA was extracted from the fecal samples using QIAamp PowerFecal Pro DNA Kit (QIAGEN, Germany). The V3-V4 region of the 16S rRNA gene was amplified from the fecal DNA samples by PCR using the following primers: forward, 5'- TCGTCGGCAGC GTCAGATGTGTATAAGCGACAGCCTACGGGNGGCWGCAG-3'; and reverse, 5'- GTCTCGTGGGCTCGGAGATGTGTATAAGAGAC AGGACTACHVGGGTATCTAATCC-3'. Library construction was performed in which the flow cell binding sequence and indexed adapters were ligated on the ends of the PCR products using for Nextera XT Index Kit v2 (Illumina, USA). The multiplexed libraries were sequenced using paired end cycles on the MiSeq with a target 130,000 reads per library and the MiSeq Reagent Kit v3 (Illumina, USA) in accordance with the manufacturer's instructions as described previously.[62] The composition of gut microbiome was determined using the EzBioCloud analytical pipeline.[63] Bray-Curtis dissimilarity analysis was conducted and presented using principal coordinate analysis (PCoA).

Reduced representation bisulfite sequencing

Sample Preparation

Genomic DNA was extracted using the MagMAX™ DNA Multi-Sample Kit (ThermoFisher 4413020) on the KingFisher Apex instrument (ThermoFisher 5400930) following manufacturer's instructions.

Library Preparation and Sequencing

100 ng of gDNA was digested with TaqaI (NEB R0149) at 65ºC for 2 h followed by MspI (NEB R0106) at 37ºC overnight. Following enzymatic digestion, samples were used for library generation using the Ovation RRBS Methyl-Seq System (Tecan 0353-32) following manufacturer's instructions. In brief, digested DNA was randomly ligated following fragment end repair and bisulfite conversion. After conversion and clean-up, samples were amplified for library construction followed by purification. Libraries were measured using Agilent 2200 TapeStation System and quantified using Nanodrop 2000c (ThermoFisher ND-2000C). Libraries were sequenced on a NovaSeq 6000 at SE75.

Single-cell RNA-sequencing

Isolation of placenta nuclei

Placenta tissues were collected on E18.5 day and stored instantly in -80°C. Placenta nuclei were dissociated using the Singulator 100 system (#100-067-764, S2 Genomics, CA, USA) with lysis buffer and 20 μL of Recombinant RNase Inhibitor (Takara Bio Inc., Shiga, Japan). The cell suspensions were filtered through a 100-μm nylon mesh cell strainer and centrifuged at 500 g for 5 min. The supernatants were discarded. The precipitate was added 500 μL 1% bovine serum albumin and hand-mixed until no precipitates. The quality and quantity of placenta nuclei were confirmed under a microscope using DAPI florescence staining.

Single-cell RNA-sequencing

Nuclei (10,000) were prepared to a concentration of 1,000 nuclei/μL and loaded into the Chromium Controller (10x Genomics), and single-cell cDNA libraries were generated using a Chromium 3′ v3 Chemistry Kit (#PN-1000075, 10x Genomics). Libraries were sequenced on a NovaSeq 6000 System (Illumina) using a NovaSeq S4 Reagent Kit (200 cycles; #20027466, Illumina).

Single-cell RNA-sequencing analysis

Raw FASTQ files were processed for each sample using the Cell Ranger software (ver 7.1.0, 10x Genomics) against the Cell Ranger mm10 mouse reference genome. Raw counts were used as the input for data processing using the Seurat R package (version 4.1.2).[64] To exclude ambient RNA contamination, the data were processed using SoupX.[65] In addition, the data were removed and considered doublets using DoubletFinder.[66] In addition, we removed cells with less than 400 detected genes, detected counts less than 1000 and more than 20,000, and mitochondrial gene content greater than 1%. Following the filtering step, we normalized nuclear genome read counts using the 'NormalizeData' function (10,000 default scale factor) separately for each dataset. We used the 'FindVariableFeatures' function to identify highly variable features for downstream analysis and integrated them using the 'FindIntegrationAnchors' and 'IntegrateData' functions. The integrated data were used for dimensionality reduction and cluster detection. We performed linear regression using the 'ScaleData' function and a linear dimensionality reduction using the 'RunPCA' function. Twenty principal components were used for downstream graph-based, supervised clustering into distinct populations using the 'FindClusters' function and uniform manifold approximation, and projection (UMAP) dimensionality reduction was performed to project the cell population onto two dimensions using the 'RunUMAP' function. Differentially expressed genes (DEGs) were detected by using the 'FindMarkers' function (log2fc.threshold > 0.25 and p_val_adj < 0.05). After retrieving the data for each cell type, we used the 'FindVariableFeatures' function to identify highly variable features for downstream analysis. We then used the 'ScaleData', 'RunPCA', 'FindClusters', 'RunUMAP', and 'FindMarkers' functions on the subsetted every cell cluster. The differentially expressed genes (DEGs) were identified according to the adjusted P values (p_val_adj < 0.05).

QUANTIFICATION AND STATISTICAL ANALYSIS

Metabolomics

General metabolite chemical classification (lipids, carbohydrates, etc.) and subpathways (fatty acid synthesis, polyunsaturated fatty acids, etc.) were determined using a combination of literature evidence and cross-references to Metabolon's internal database. Statistical analyses, including principal component analysis and analysis of variance (ANOVA), were carried out using Metabolon's Integrated Bioinformatics Platform and MetaboAnalyst 6.0.[54] A full list of metabolites and metrics is shown in Table S1.

Integrated metabolic pathway analysis

Pathway analysis integrating gene and metabolite enrichment was performed using the Joint Pathway Analysis tool in MetaboAnalyst 6.0.[54]

Circadian Rhythmicity Determination

A time series of expression levels was used to determine the circadian behavior of the transcripts using the cosinor method. Daily rhythmicity of transcripts and metabolites from RNA-seq and the metabolome was assessed using the non-parametric JTK-CYCLE algorithm incorporating a 24 h period.[55] Transcripts with no detectable expression/abundance in more than six biological replicates were filtered out before rhythmicity was tested. Genes and metabolites were considered rhythmic over the circadian cycle if their permutation-based, adjusted p-values were <0.05.

Bioinformatic Analysis

The Database for Annotation, Visualization and Integrated Discovery (DAVID) pathway analysis tool was used to identify GO terms related to biological processes (https://david-d.ncifcrf.gov/).[56] Differential analysis of gene expression at individual ZTs was carried out using Cyber-T.[57,58] Transcripts with no detectable expression/abundance in more than six biological replicates were filtered out before the downstream analysis was performed. The analysis was performed using pipelines implemented for the Circadiomics[59,67,68] database and web portal (circadiomics.ics.uci.edu).

Other Statistical Analyses

Experimental data were presented as means + standard error of mean (SEM) unless otherwise specified. The points where the error bars were shorter than the height of the symbol, the error bars were not drawn. Comparisons between two groups were conducted using student's *t* test or Mann-Whitney test. Kruskal-Wallis test was used to compare the four groups of amplitude distribution in the diurnal metabolome and transcriptome. Two-way ANOVA with the Sidak post-hoc test was performed when groups on two different variables were compared (GraphPad Prism 10). In qPCR, any data more than 1.5 interquartile ranges above the third quartile or below the first quartile were defined as outliers and were excluded from the analysis. Heat maps of the rhythmic transcripts were generated by R package 'gplots'. Polar histograms were generated by R package 'ggplot2'. Graphs were constructed using Microsoft Excel, GraphPad Prism 10, and Adobe Illustrator 2023, RStudio. Differentially expressed genes with p_val of 0 in the single cell RNA-seq of the placenta were not presented in the volcano plots in Figure 6J. The Figure was partly generated and adapted from "Activity-Based Anorexia (ABA) Timeline", "Transgenic Mice Production (Microinjection)", "Mice Breeding Technique", and "Tamoxifen-Induced Gene Deletion in Mouse Model" by BioRender.com (2023). Retrieved from https://app.biorender.com/biorender-templates.